REVIEW

Check for updates

Trends in molecular design strategies for ambient stable n-channel organic field effect transistors

Joydeep Dhar, [ID] [a] Ulrike Salzner [ID] [b] and Satish Patil [ID] *[a]

In recent years, organic semiconducting materials have enabled technological innovation in the field of flexible electronics. Substantial optimization and development of new π-conjugated materials has resulted in the demonstration of several practical devices, particularly in displays and photoreceptors. However, applications of organic semiconductors in bipolar junction devices, *e.g.* rectifiers and inverters, are limited due to an imbalance in charge transport. The performance of p-channel organic semiconducting materials exceeds that of electron transport. In addition, electron transport in π-conjugated materials exhibits poorer atmospheric stability and dispersive transient photocurrents due to extrinsic carrier trapping. Thus development of air stable n-channel conjugated materials is required. New classes of materials with delocalized n-doped states are under development, aiming at improvement of the electron transport properties of organic semiconductors. In this review, we highlight the basic tenets related to the stability of n-channel organic semiconductors, primarily focusing on the thermodynamic stability of anions and summarizing the recent progress in the development of air stable electron transporting organic semiconductors. Molecular design strategies are analysed with theoretical investigations.

1. Introduction

The last few decades have witnessed enormous progress towards realization of printed organic electronics. Research on conjugated π-systems intensified with the discovery of the sharp increase in the electrical conductivity of polyacetylene after exposing it to vapours of chlorine, bromine or iodine. Alan J. Heeger, Alan G. MacDiarmid, and Hideki Shirakawa were awarded the Nobel Prize in Chemistry in 2000 for the discovery and development of conductive polymers.[1,2] Rapid progress in materials design and synthesis concomitant with a continuous increase in fundamental understanding has established the field of organic electronics. Commercialization of organic

[a] *Solid State and Structural Chemistry Unit, Indian Institute of Science, Bangalore 560012, India. E-mail: satish@sscu.iisc.ernet.in; Fax: +91-80-23601310; Tel: +91-80-22932651*
[b] *Department of Chemistry, Bilkent University, 06800 Bilkent, Ankara, Turkey*

Satish Patil is presently an Associate Professor at Indian Institute of Science, Bangalore. He received his PhD in polymer chemistry at the Bergische University of Wuppertal, Germany under the guidance of Prof. Ullrich Scherf. He then moved to the laboratory of Prof. Fred Wudl at University of California Los Angeles (UCLA) as a California Nanosystem Institute Post-doctoral fellow (CNSI). In 2006, Dr Satish Patil was appointed as an Assistant Professor in the solid state and structural chemistry unit at Indian Institute of Science, Bangalore. His research interests currently focus on synthesis of conjugated polymers and small molecules for organic electronics.

Satish Patil

Joydeep Dhar completed his Masters in Chemistry from Indian Institute of Technology (IIT) Madras in 2009. Then in 2015, he received his PhD from Indian Institute of Science (IISc) Bangalore under the supervision of Prof. Satish Patil. His thesis was focused on structure-property correlation of selenium based organic semiconductors. Currently he is working as Dr D. S. Kothari Postdoctoral Fellow in Jadavpur University, Kolkata, India.

Joydeep Dhar

7404 | *J. Mater. Chem. C*, 2017, **5**, 7404–7430

This journal is © The Royal Society of Chemistry 2017

semiconductors (OSCs) began with their utilization as photoconductors in copiers and laser printers, in organic light emitting diodes (OLEDs), and as antistatic coatings.[3–6] The demand for developing efficient π-conjugated organic molecules has increased manifold, especially because of their ability to coat most substrates with high mechanical robustness, maintaining their rheological properties.[7–10] Therefore emphasis lies on inexpensive synthetic procedures and improved solution processability. The ultimate goal is the fabrication of large area roll-to-roll (R2R) printable electronic devices in a cost-effective manner as an alternative to conventional silicon-based technologies.[11–14]

Organic field effect transistors (OFETs) are versatile devices for a variety of applications including radio-frequency identification tags (RFIDs), flexible active-matrix displays, electronic paper, electronic skin, and sensors.[10,15–19] Moreover, OFETs constitute important parts of integrated circuits (ICs) which are the backbone of modern electronic circuitry.[20] Since the first demonstration of an OFET in 1986,[21] the transport properties of a plethora of OSCs were measured in OFET devices and their applicability in electronic devices was demonstrated.[20,22–25] The performance of organic semiconductors in OFETs has improved steadily over the last decade. Charge carrier mobility (μ), defined as the drift velocity under unit potential gradient, is the most important parameter to fabricate high performance OFET devices.

Depending on the nature of the charge carriers, OSCs can be divided into two categories, p-channel (hole transporting) and n-channel (electron transporting). Recently, the hole mobilities of organic thin film transistors have improved dramatically and now exceed those of thin-film amorphous silicon devices.[26–31] However, the steady and fast improvement in p-channel mobility has outperformed n-channel mobility, especially in terms of device stability.[32] The imbalance between hole and electron mobility severely limits the applicability of OSCs in bipolar electronic devices such as low power complementary ICs, inverters, and OPVs for which balanced p- and n-channel charge carrier mobilities are a primary requisite. As there is no principal physical difference between electron and hole transport,[33] the

observed lower n-channel mobilities are most likely due to higher barriers to charge injection, lower stability of the reduced state compared to the oxidized state, the presence of electron traps created by oxygen and water molecules,[33–36] and intrinsic charge carrier trapping caused by localization in the conduction band.

Conjugated polymers have the potential to conduct electrons and holes much better than small molecules because mobility along the conjugated chain can be very high. The on chain mobilities of holes were shown to reach 600 cm^2 V^{-1} s^{-1} in long, planar ladder-type oligomers.[37] However, in terms of long range transport, small molecules outperform polymers because of their better crystallinity and more suitable morphology. The mobilities of holes in ultrapure naphthalene crystals were shown to be as high as 400 cm^2 V^{-1} s^{-1} being limited only by experimental restrictions.[38] The electron mobilities in perylene crystals are lower but reach 100 cm^2 V^{-1} s^{-1}.[38] Unfortunately, morphology is a crucial issue that can cause orders of magnitude changes in mobility in devices made of the same material depending on the processing conditions.[39]

Realistic modeling of long-range transport through organic materials is extremely complicated, as it requires accurate calculation of intramolecular and intermolecular coupling and must take structural and dynamical disorder into account.[34,40–52] Theoretically predicted electron mobilities of idealized materials without disorder are therefore upper bounds for the highest possible mobility and should not be expected to reproduce experimental values. Intramolecular transport through a long, π-conjugated system is coherent band-like as confirmed by increasing conductivity with decreasing temperature.[37] Transport through ultrapure single crystals was likewise shown to be coherent band-like.[38]

The instability of n-channel charge carriers in air poses a serious bottleneck in using OSCs under ambient conditions.[53] In recent years, a lot of attention has been focused on developing n-channel and ambipolar OSCs with new design principles utilizing the basic understanding of electron transport and electrochemical stability criteria.[54] Hence, optimizing the n-channel transport requires insights into intrinsic transport properties combined with experimental optimization. Therefore, we are reviewing experiment and theory side by side and compare theoretical and experimental studies where available. Our analysis reveals the strength and limitations of theoretical predictions and we demonstrate that the predictive power of relatively simple theoretical approaches is remarkable. The focus is on n-channel molecular materials with superior charge transport properties which are stable under ambient conditions. Furthermore, we highlight synthetic strategies adopted to enhance the air stability of n-channel transistors.

2. Basic principles for observing n-channel mobility in OSCs

Friend and co-workers demonstrated by using trap-free dielectrics that, in principle, π-conjugated materials are capable of transporting both holes and electrons, but only under inert testing conditions.[36] Besides trap states, other intrinsic and extrinsic factors such as
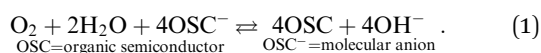
Ulrike Salzner was born in 1960 in Nürnberg, Germany. She studied chemistry at the University of Erlangen and received her doctorate under Prof. Paul v. R. Schleyer. She did post-doctoral work at Northern Illinois University, USA and at Memorial University of Newfoundland, Canada. After that she joined Bilkent University, Ankara, Turkey where she works as a full professor. Her research interests currently focus on theoretical investigation of optical and electronic properties of materials for organic electronics.
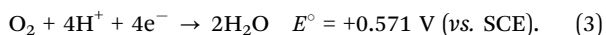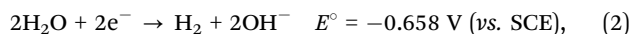
Ulrike Salzner

oxidation by oxygen from air or by water molecules[55] are responsible for diminishing n-channel mobilities.[53] In contrast, p-channel materials are less susceptible to oxidation and proved to be robust under ambient conditions. The steady improvement of the hole mobility of π-conjugated organic materials is primarily due to stabilization of polarons in electron-rich backbones. Ionization energies (IEs) that are close to the work functions of commonly used air-stable metals such as Au, Ag, and Pt facilitate hole injection with a minimum energy barrier. In contrast, electron injection from Au or Ag electrodes into the LUMO is energetically unfavorable due to the energy mismatch between the metal work function and electron affinity (EA) of OSCs. Low work function metals, such as Mg, Ca, or Al, cannot be used as they are notoriously sensitive towards air oxidation and react with the semiconductors.[56]

Moreover, oxidation of OSC anions in the presence of water and oxygen poses a major hurdle to develop air-stable n-channel materials for OFETs.[55] The anion formed after electron injection in the semiconducting channel of OFETs is readily oxidized by moisture or oxygen as shown below in eqn (1).

$$O_2 + 2H_2O + 4OSC^- \rightleftharpoons 4OSC + 4OH^- \quad . \quad (1)$$
$$\underset{OSC=organic\ semiconductor}{} \quad \underset{OSC^-=molecular\ anion}{}$$

Hydroxide ion also act as trapping centres limiting the n-channel performance. The majority of n-channel semiconductors operate only under an inert atmosphere, with decreasing performance under ambient conditions. It has been demonstrated that n-channel transport can be regained under inert conditions.[57] This proves that the difficulty in developing n-channel semiconductors lies in the inherent reactivity of the anions and not in the chemical instability of the semiconductors in their neutral forms. Hence, one of the design principles for making robust n-channel semiconductors relies upon preventing oxygen or moisture from penetrating into the molecular backbone. Typically, in recent years new molecular design strategies have been followed to optimize thermodynamic and kinetic factors related to stability issues with the anions of OSCs.

To ensure thermodynamic stability of a molecular anion, the EA of the neutral material has to be above 4 eV.[55,58] The EA and reduction potential can be correlated according to eqn (2) and (3).

$$2H_2O + 2e^- \rightarrow H_2 + 2OH^- \quad E^\circ = -0.658\ V\ (vs.\ SCE), \quad (2)$$

$$O_2 + 4H^+ + 4e^- \rightarrow 2H_2O \quad E^\circ = +0.571\ V\ (vs.\ SCE). \quad (3)$$

If the reduction potential is ≥ -0.658 V (vs. SCE) or the EA of the neutral species is above 3.84 eV, the anion is thermodynamically stable against oxidation by moisture. To prevent oxidation of an anion by O_2, its reduction potential must be higher than +0.571 (vs. SCE). There are electron deficient organic materials whose reduction potentials exceed −0.658 V (vs. SCE) but organic semiconductors with reduction potentials greater than +0.571 V (vs. SCE) are extremely rare and hence, all molecular anions are thermodynamically unstable toward air oxidation. Nevertheless, experimental evidence suggests that there exists an over potential (activation energy barrier) for the

oxidation by O_2 of 0.9–1.0 V which brings the stability window near EAs of 4.0 to 4.1 eV. Hence, increasing EAs by judicious material design to around 4.0 eV is a promising and feasible solution for developing an air stable n-channel and in turn ambipolar materials for OFET applications. Chao and co-workers have determined the minimum value of EA to be 2.8 eV to achieve ambient-stable n-channel operation from theoretical calculations on a large number of organic semiconductors.[59] Therefore, inclusion of strong electron withdrawing groups to enhance the EA is a simple but effective approach to develop ambient stable n-channel organic semiconductors. The EAs should not be too large, however, as organic molecules with EAs above 4.5 eV are prone to unintentional n-doping, leading to loss of semiconducting properties. Although the EA is the parameter that indicates the propensity of a molecule to get reduced, it is common practice to correlate the thermodynamic stability of anions with the LUMO energy levels of the corresponding neutral species.[60] Thus, throughout the manuscript the LUMO level is also considered as a parameter for material stability for observing n-channel operation.

Besides thermodynamic considerations, various kinetic parameters are important for achieving ambient stability of n-channel operation. There are a number of examples where kinetic factors related to the different device elements become important for improving open air electron transport properties. These factors do not influence the stability of the molecular anion, but minimize the interaction between atmospheric oxidants and the additional electrons in the reduced state of the organic semiconductor. Un et al. have demonstrated that the chemical stability of dielectrics in FET devices is as important as the electrochemical stability of the semiconductors.[61] The active hydrogen at the surface of dielectrics such as SiO_2 creates electron trapping centres by reacting with OH^- generated according to eqn (2). Therefore passivation of the dielectric with silane derivatives, e.g. OTS, OTMS, and HMDS, reduces the number of trapping sites at the SiO_2/semiconductor interface and enhances n-channel performance.[62,63] These materials render the SiO_2 layer hydrophobic by reacting with the silanol groups (SiOH) present at the surface. Dielectric surface modifiers decrease the surface energy and increase the smoothness of the surfaces which improves the crystallinity of the deposited thin films, increases the grain-sizes, and concomitantly reduces the number of grain boundaries.[64] Organic thiol based self-assembled monolayers (SAMs) can be deposited on the electrodes to reduce contact resistance and to facilitate electron injection.[65] The observed performance improvements were attributed to the formation of interfacial dipoles which align to form a favourable energy band structure, enhancing electron injection and effectively blocking the counter ions. As electron mobilities vary for the same OSCs with different dielectric materials, proper selection of the dielectric is critical for fabricating air stable n-channel OFET devices.[62,66,67] This might be due to energetic disorder at the dielectric/semiconductor interface induced by dipolar disorder in the dielectric layer, which increases with increasing dielectric constant, κ.[68] The dielectric constant of the material should, however, be high enough for providing sufficient charge carrier

7406 | J. Mater. Chem. C, 2017, 5, 7404–7430

This journal is © The Royal Society of Chemistry 2017

concentration in the OFET channel. SiO$_2$ (κ = 3.9) is a common choice of dielectric in OFETs, but it is unsuitable for n-type charge transport without surface treatment because hydroxyl groups at the SiO$_2$ surface act as electron trapping centres as mentioned before. Hence, different hydrophobic organic dielectrics such as CYTOP, BCB, PS, and PMMA are used frequently when ambient stable n-channel transport is expected.[14]

The n-type charge carrier mobility of an OSC and its ambient stability also depends upon device fabrication procedures; the way the semiconductor is deposited and processed, and the device geometry which is adopted.[69] There are several reports which corroborate the influence of thin film morphology on the charge transport properties in OSCs.[70,71] Not only device performance but also stability is directly related to the thin film morphology. Wen et al. studied the effect of film growth rate on morphology.[72] Superior charge carrier mobilities are observed for thin film devices with larger grains, obtained with slow growth rates. Effects on stability are more complicated as varying growth rates during film formation may lead to films with better air stability. This can be explained by the fact that physisorption of moisture or oxygen occurs at grain boundaries.[62,73] If the grain boundaries reach deep into the material, moisture or oxygen can penetrate into the semiconductor and reach the semiconductor–dielectric interface acting as electron-trapping centres. Varying the growth rate allows larger molecules to fill the gaps of the layer below, reducing the number of grain boundaries. In another study, Weitz and co-workers observed differences in charge carrier mobilities and stability between single-crystalline ribbons and polycrystalline thin films.[70] Single-crystalline ribbons show higher electron mobility and better atmospheric stability than vacuum deposited thin films because they have fewer grain boundaries. Therefore, control over thin film morphology improves the device performance as poor morphology causes mobility below its intrinsic value. Thermal annealing of the OSCs is a common procedure for improving the molecular packing, planarity, order, and crystallinity of thin films.[74,75] Most OSCs reach their best mobility values only after annealing at an optimal temperature. Thin film annealing procedures and associated electrical performance of an OSC were correlated by Kim et al.[76] Furthermore, removing the residues of a polar solvent with heat treatment assists in achieving higher electron mobilities.[77] Thin film morphology is also dependent on the method of film preparation. Deposition

techniques, such as drop-casting, spin-coating, ink jet printing, thermal evaporation, and solution shearing, are applied to prepare high quality thin films with precise control over film thickness.[78,79] In thermally evaporated thin film devices, variation in deposition pressure changes the thin film morphology significantly.[80] Bao and coworkers investigated the charge transport properties of some molecular OSCs and found that thin films prepared by solvent-shearing have improved orientation of the molecules with short interplanar distances, resulting in higher n-type mobilities compared to devices fabricated using drop-casting or spin-coating.[81–83] The influence of device geometry on the type and amplitude of charge carrier mobilities and especially the stability of the n-channel transport were reported by several research groups.[84] Better performance of top-gated devices is frequently observed and rationalized by easier injection of charges from the source-drain electrodes as the larger active electrode area reduces contact resistance.[85,86] Top-gate OFET devices have also better stability under ambient conditions because the active layer is sandwiched in between the substrate and dielectric layers, preventing direct air exposure of the OSC.[14]

Apart from device parameters, the stability of the molecular anions can also be enhanced by hindering the ingress of oxygen and moisture into the molecular backbone with rational molecular design. This is achieved by functionalizing the π-conjugated aromatic backbone with halogen atoms, mainly fluorine, to create a kinetic barrier.[87] Fluorination also increases the hydrophobicity of organic materials. Since fluorine is very small and leads to strong hydrogen bridging, substitution with fluorine may additionally improve the structural features and strengthen the molecular organization. A compact molecular arrangement enhances electron transport by increasing charge transfer integrals. Fig. 1 depicts the effect of thermodynamic and kinetic control in achieving the air-stable n-channel OFET which will be highlighted with a few examples of efficient molecular n-channel semiconductors in the following sections.

3. Theoretical methods for investigating electron transport

The ultimate goal of theory in the field of organic electronics is to predict device performance from the material structure.[88]
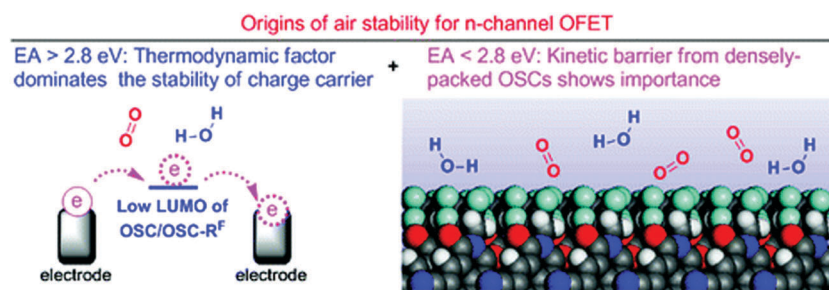

Fig. 1 The origin of air-stable n-channel operation has been shown pictorially from the viewpoint of thermodynamic and kinetic parameters (adapted from ref. 59).

This goal has not been achieved yet because apart from computing the intrinsic electronic properties of the material this requires predicting the crystal structures,[89,90] accounting for anisotropy,[91] including molecular vibrations,[92] and correctly assessing the amount of structural and dynamic disorder. Research on disorder is picking up momentum[93–97] but the majority of studies are concerned with the intrinsic electronic properties[98–102] of idealized materials.

Coherent transport in highly ordered materials can be calculated by applying the Landauer formula[103] or various other flavors of scattering theory.[92,104,105] With increasing temperature, dynamic fluctuations rather than impurities induce localization.[42,106] Conductivity then increases with increasing temperature because hopping transport is temperature activated. In the high temperature regime, when localization is significant compared to electronic coupling, polaron (Marcus–Holstein) models[107–109] are applicable. Key parameters for Marcus theory are reorganization energies (λ) and charge transfer integrals (τ) which measure the strength of the interaction of neighbouring molecules. Mobility further depends on the temperature (T) and travelling distance (r) of the charge carrier.[34] Hopping models do not apply, however, when the charge transfer integrals are greater than half of λ.[43] Already close to but especially beyond this limit, Marcus theory greatly exaggerates mobility values. Using realistic values of T and r and varying τ shows that mobilities in one direction should not exceed ~ 1 cm^2 V^{-1} s^{-1} for hopping models to be valid (Fig. 2). The validity of the hopping approach has to be evaluated carefully[43,45,110] also because grain boundaries may lead to apparent temperature activated transport even if transport is band-like within the grains.[111]

Crucial intrinsic material properties that facilitate electron conductivity in organic materials apart from stability of the reduced state are: extent of the π-conjugation in the anionic state which requires planarity, strong interactions within and between oligomers; small λ upon reduction; and suitable energy levels relative to those of the source and drain electrodes to facilitate efficient charge injection. These parameters can be determined reliably using density functional theory (DFT).

Despite all the progress using DFT, there is no single density functional that works for all properties and systems.[112–118] There is not much difference between the predictions with different correlation functionals as the most important parameter for determining the properties of conjugated systems is the amount of Hartree–Fock (HF) exchange. Increasing the amount of HF-exchange decreases defect sizes, increases spin-contamination,[119] increases λ,[99] and increases τ.[120] Because of the variety of polaron sizes from different theoretical methods and the strong influence of disorder in experiments, the exact polaron size remains a long standing problem in organic electronics research. The reorganization energy for electron transport (λ^-) is the difference between adiabatic and vertical electron affinities of the neutral species plus the difference between vertical and adiabatic ionization energies of the anion. Fine tuning of the amount of HF-exchange required to reproduce experimental λ-values leads to values between 23.99 and 36.39% depending on the functional employed.[121] τ can be assessed using several methods, e.g. the energy-splitting-in-dimer approach,[34] site energy correction,[122] and the direct coupling method.[123] The simplest of the three, the energy-splitting-in-dimer method, however, tends to underestimate τ.[124] As mobilities increase with increasing τ and decreasing λ while both increase with HF-exchange, it is possible to manipulate the predicted mobilities by calculating λ and τ with different density functionals.[99] However, as the measured mobilities differ by orders of magnitude depending on the processing conditions,[39] forcing agreement between theory and experiment leads to little insight.

Therefore, DFT methods are extremely useful for predicting trends between systems but are problematic for absolute numbers. As trends are reproduced reasonably well with most functionals, the choice of the density functional is not crucial for general assessments. The common practice to use (incorrect) B3LYP orbital energies as IEs, EAs, and redox potentials, and to predict optical gaps from orbital energies can be justified as trends in these properties are reproduced fairly well. The use of Marcus theory in transport calculations must be viewed with a grain of sand as the high measured mobility values of ultrapure crystals indicate that intrinsic transport in these systems is coherent.
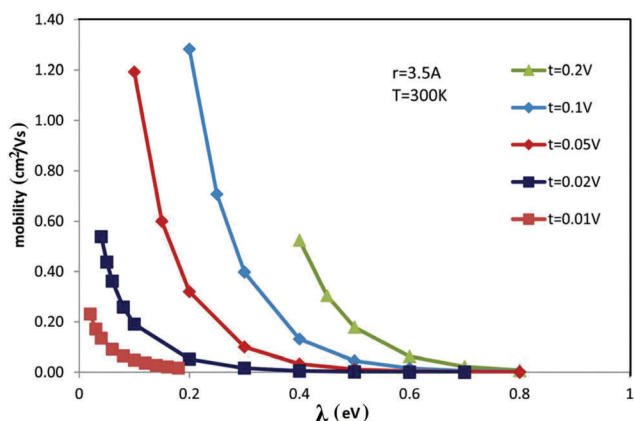

Fig. 2 Single path mobilities predicted using Marcus theory. The curves end at $\lambda = 2\tau$, the limit for Marcus theory to be applicable.

4. Representative examples of n-channel molecular semiconductors

In the early nineties, n-channel charge transport was observed for the first time in small molecules based on metal phthalo-cyanines.[125] In 1996, Horowitz and co-workers measured n-channel mobility of the order 10^{-5} cm^2 V^{-1} s^{-1} for perylene diimide based OSCs.[126] Tetracarboxylic diimides were recognized as prototypical, because they fulfil the primary requirements for electron transport with high environmental stability because of their large EAs and strong intermolecular π–π interactions.[126–130] Among the diimide derivatives, perylenetetracarboxylic diimide (PDI) and naphthalenetetracarboxylic diimide (NDI) seem to be the most suitable for electron transporting OSCs.[129,131–135] Meanwhile, additional strategies were adopted following basic

7408 | J. Mater. Chem. C, 2017, 5, 7404–7430

This journal is © The Royal Society of Chemistry 2017

tenets for electron injection, stabilization and transportation through the molecular backbone of π-conjugated OSCs.[34,136] In the next section, we will illustrate the continuing effort devoted to developing environmentally stable n-channel molecular materials based on electron withdrawing imide, cyano, carbonyl, and halogen substituted small molecule semiconductors.

4.1 Diimide derivatives

Diimide derivatives show stable n-channel characteristics as they possess relatively high EAs due to the strong electron withdrawing effect of the imide moiety. The disadvantages of unsubstituted diimide molecules are that they are sparingly soluble and their LUMOs lie at only around −3.6 eV.[137] Therefore, further functionalization is necessary to lower the LUMOs into the thermodynamic stability region and to increase their solubilities. A common practice is to functionalize at the N-atoms to improve the solubility and to induce lamellar packing and/or at the core position to extend the π-conjugation. Enhancing molecular packing improves the charge transport properties of NDI and PDI derivatives. Examples of N- and core-substituted NDI derivatives of naphthalenetetra-carboxylic dianhydride are shown in Fig. 3. These high mobility NDI derivatives are highlighted to illustrate the influence of substituents on lowering the LUMO energy.

The NDI based molecule 1a with *n*-hexyl substituents at the N-atoms exhibits an n-channel FET mobility of 0.7 cm^2 V^{-1} s^{-1} and a current on/off ratio of 6 × 10^6 under argon (Ar) atmosphere (Table 1).[138] As compared to linear *n*-hexyl chains, cyclohexyl substituents dramatically increase the thin film electron mobility from 0.70 (1a) to 6.2 cm^2 V^{-1} s^{-1} (1b) under argon (Ar) due to improved intermolecular π–π stacking interactions.[138] The shortest π–π stacking distance for 1b is 3.34 Å whereas large π–π distances of 4.9 Å were determined for 1a using single crystal X-ray diffraction. For 1b, powder X-ray diffraction patterns of thermally evaporated thin films indicate a similar packing arrangement to that of single crystals grown

using the train sublimation technique. This explains the large differences in n-channel mobility between the two NDI derivatives 1a and 1b with different *N*-alkyl substituents. The thin film mobility of 1b was further improved to 7.5 cm^2 V^{-1} s^{-1} after equilibrating under Ar for 30 min at low humidity. A slightly reduced mobility of 5.5 cm^2 V^{-1} s^{-1} was recorded in humid air. The n-channel mobility decreased to 0.41 cm^2 V^{-1} s^{-1} at higher humidity (60%) in the presence of oxygen. To improve the electron mobility and air stability of NDI derivatives, kinetic effects of *N*-fluoroalkyl or fluorophenyl substituents are utilized. Fluoroalkyl substituted 1c shows an n-channel mobility of 0.34 cm^2 V^{-1} s^{-1} when tested in N$_2$ and 0.27 cm^2 V^{-1} s^{-1} in air.[139] Single crystal OFET devices based on 1c exhibit improvement in charge carrier mobility to 0.7 cm^2 V^{-1} s^{-1} under vacuum.[140] Enhanced ambient stability was proved with n-channel mobilities of 0.7 cm^2 V^{-1} s^{-1} of NDI derivative 1d which is substituted with longer *N,N′*-fluoroalkyl chains.[141] Two NDI derivatives, 1e with a single trifluoromethyl substituent at the 4 position of the benzyl group and 1f with two trifluoromethyl groups at the 3 and 5 positions, show similar electron mobilities with air stability, though 1e packs in a herringbone fashion while 1f has NDI cores that are oriented parallel.[135,142] In air, both compounds exhibit n-channel mobilities of 0.12 cm^2 V^{-1} s^{-1} and a high current on/off ratio of 10^6–10^7 on octadecyltrimethoxysilane (OTMS) treated Si/SiO$_2$ substrates in bottom-gate top-contact devices. For 1f, the mobility marginally improves to 0.15 cm^2 V^{-1} s^{-1} when the SiO$_2$ substrate is treated with perfluorodecyltriethoxysilane (PFOS). Changing the *N*-substituent from benzyl in 1f to phenyl in 1g, slightly enhances the electron mobility.[143] The best value of 0.24 cm^2 V^{-1} s^{-1} was measured for compound 1g under a nitrogen atmosphere. Like 1f, compound 1g is stable in air. During 42 days of storage in air, the mobility reduces to 0.13 from 0.15 cm^2 V^{-1} s^{-1} under nitrogen. Meng and co-workers have replaced p-CF$_3$ in 1e with a trifluoromethoxy (OCF$_3$) group, since OCF$_3$ is a stronger electron-withdrawing and π-donating

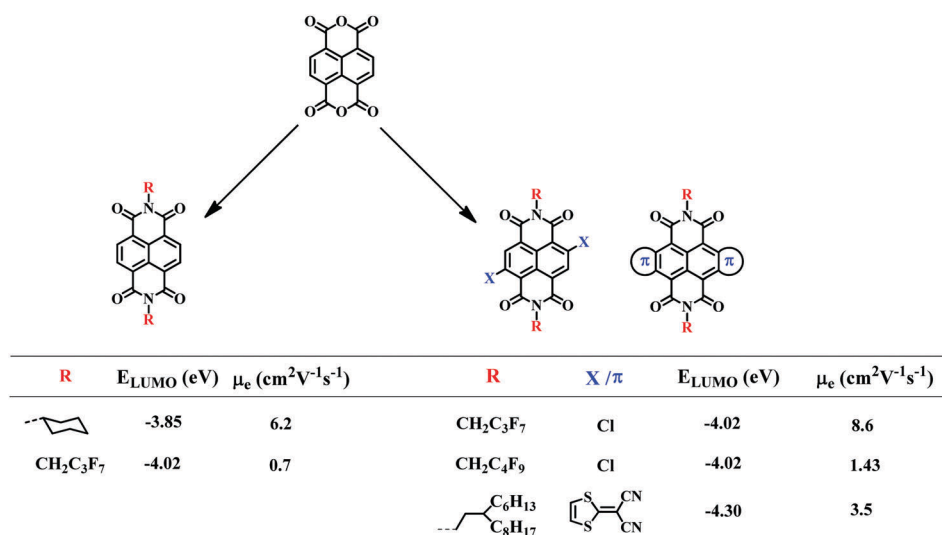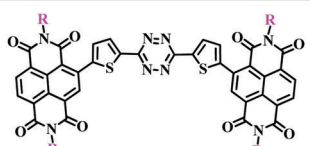| R	E$_{LUMO}$ (eV)	μ$_e$ (cm^{2}V^{-1}s^{-1})	R	X /π	E$_{LUMO}$ (eV)	μ$_e$ (cm^{2}V^{-1}s^{-1})
cyclohexyl	-3.85	6.2	CH$_2$C$_3$F$_7$	Cl	-4.02	8.6
CH$_2$C$_3$F$_7$	-4.02	0.7	CH$_2$C$_4$F$_9$	Cl	-4.02	1.43
			C$_6$H$_{13}$ C$_8$H$_{17}$	thiophene-CN/CN	-4.30	3.5

Fig. 3 Synthesis of differently substituted NDI derivatives. The influence of N- and core substituents on LUMO energy and electron mobility is demonstrated.

Table 1 Representative examples of n-channel NDI derivatives and the corresponding device parameters

Chemical structures		R	X/π_1	Y/π_2	E_{LUMO} (eV)	μ (cm^2 V^{-1} s^{-1})	$I_{on/off}$	Device structures	Ref.
	1a	C_6H_{13}	H	H	−3.85	0.7 (Ar)	10^5	BGTC; Au; Si/SiO$_2$; OTMS	138
	1b	[cyclohexyl]	H	H	−3.85	6.2 (Ar, 22% RH)	10^8	BGTC; Au; Si/SiO$_2$; OTS	138
						0.41 (O$_2$, 60% RH)	10^6		
	1c	$CH_2C_3F_7$	H	H	−4.01	0.34 (N$_2$)	10^5		139
					−4.02	0.27 (air)	10^6		
						0.7 (sc)		BGTC; Au; Si/SiO$_2$; OTS	140
	1d	$C_3H_6C_8F_{17}$	H	H	−3.71	0.7 (air)	10^6	BGTC; Au; Si/SiO$_2$; OTS	141
	1e	[aryl–CF$_3$]	H	H		0.12 (air)		BGTC; Au; Si/SiO$_2$; OTMS	135
	1f	[aryl(CF$_3$)$_2$]	H	H		0.15 (air)	10^7	BGTC; Au; Si/SiO$_2$; PFOS	142
	1g	[aryl(CF$_3$)$_2$]	H	H	−4.09	0.15 (N$_2$)	10^5	BGTC; Au; Si/SiO$_2$; OTS	143
						0.13 (air)	10^5		
	1h	[aryl–OCF$_3$]	H	H	−4.22	0.7 (air)	10^6	BGTC; Au; Si/SiO$_2$; OTS	144
	1i	[aryl–SCF$_3$]	H	H	−4.03	0.17 (air)	10^6	BGTC; Au; Si/SiO$_2$; OTS	145
	1j	[aryl–C$_2$H$_4$C$_8$F$_{17}$]	H	H		0.57 (air)	10^5	BGTC; Au; Si/SiO$_2$; OTS	142
	1k	[C$_6$F$_5$–CH$_2$]	H	H		0.87 (vacuum)	10^7	BGTC; Au; Si/SiO$_2$; PαMS	146
						0.31 (air)	10^7	BGTC; Au; Si/SiO$_2$; OTS	
	1l	$CH_2C_3F_7$	Cl	H	−4.01	4.26 (vacuum)	10^6	BGTC; Au; Si/SiO$_2$; OTES	148
						8.6 (sc, air)	10^7	BGTC; Au; Si/SiO$_2$; OTES	147 and 149
						0.91 (air)	10^6	BGTC; Au; Si/SiO$_2$	139
	1m	$CH_2C_4F_9$	Cl	H	−4.01	1.26 (N$_2$)	10^7	BGTC; Au; Si/SiO$_2$; OTS	139
						1.43 (air)	10^7		
	1n	C_8H_{17}	CN	H	−4.5	0.11 (air)	10^3	BGTC; Au; Si/SiO$_2$; OTS	58
	1o	C_8H_{17}			−3.79	0.35 (vacuum)		BGTC; Au; Si/SiO$_2$; HMDS	151
						0.1 (air)			
		$R_1 = R_2$	$\pi_1 = \pi_2$						
	1′a	[C$_{10}$H$_{21}$/C$_8$H$_{17}$]	[thiazole–(CN)$_2$]		−4.36	1.2 (air)	10^7	BGBC; Au; Si/SiO$_2$; PFBT	152
	1′b	[C$_6$H$_{13}$/C$_8$H$_{17}$]	[thiazole–(CN)$_2$]		−4.3	3.5 (air)	10^7	BGBC; Au; Si/SiO$_2$; OTS	84
	1′c	C_8H_{17}	[thiophene–Cl]		−4.1	0.73 (air)	10^5	BGTC; Au; Si/SiO$_2$; ODTS	153
	1′d	C_8H_{17}	[thiophene–imidazole]		−4.1	0.025 (air)	10^4	BGTC; Au; Si/SiO$_2$; ODTS	153
	1′e	[C$_{10}$H$_{21}$/C$_8$H$_{17}$]	[thiazole–(CN)$_2$] [thiazole–thiophene]		−4.35	0.17 (air)	10^6	BGBC; Au; Si/SiO$_2$; PFTP	154
		R_1	R_2	$\pi_1 = \pi_2$					
	1′f	[C$_{10}$H$_{21}$/C$_8$H$_{17}$]	[aryl–C(CH$_3$)$_3$]	[thiazole–(CN)$_2$]	−4.32	0.7 (air)	10^7	BGTC; Au; Si/SiO$_2$; OTS	155
	1′g	C_6H_{13}			−4.72	0.96 (air)	10^7	TGBC; Au; Si/SiO$_2$/CYTOP	156

Table 1 (*continued*)

Chemical structures	R	X/π_1	Y/π_2	E_{LUMO} (eV)	μ (cm^2 V^{-1} s^{-1})	$I_{on/off}$	Device structures	Ref.
	1'h C$_6$H$_{13}$				0.17 (air)	10^4	TGBC; pAg; Al$_2$O$_3$/CYTOP	157

OTMS: octadecyltrimethoxysilane, OTS: octyltrichlorosilane, PFOS: perfluorodecyltriethoxysilane, ODTS: octadecyltrichlorosilane, HMDS: hexamethyldisilazane, TPA: tetradecylphosphonic acid, β-PTS: β-phenyltrichlorosilane, PFBT-perfluorobenzenethiol, PFTP: pentafluorothiophenol, BGTC: bottom-gate top-contact, BGBC: bottom-gate bottom-contact, TGBC: top-gate bottom-contact.

substituent than the CF$_3$ unit.[144] This results in improvement in open air n-type mobility from 0.12 to 0.7 cm^2 V^{-1} s^{-1} for compound **1h**. Interestingly, the (trifluoromethoxy)phenyl (C$_6$H$_5$OCF$_3$) substituted NDI derivative shows non-detectable n-channel activity, though it has a similar LUMO position to that of **1h**. Higher τ value for the LUMO level with well-defined thin film morphology having larger grains ($\sim$2 μm) and enhanced crystallinity is believed to be responsible for better electron transport of **1h**. With the aim of improving the ambient stability further, a trifluoromethanesulfenyl (SCF$_3$) group in place of OCF$_3$ was incorporated leading to the new n-type molecular semiconductor **1i** with enhanced lipophilic properties.[145] In a comparative study, it was shown that **1i** has improved open air device stability compared to **1e** and **1h**, but that n-channel mobility decreased to 0.17 cm^2 V^{-1} s^{-1}. Since **1h** and **1i** have similar crystal packing with comparable τ values for the LUMOs, the drop in efficacy of n-channel operation for **1i** was rationalized by poorer thin film crystallinity and discontinuous film morphology. Replacing the p-CF$_3$ substituent on the *N,N'*-benzyl groups of **1e** with n-CH$_2$CH$_2$C$_8$F$_{17}$ in **1j** enhances the open air mobility from 0.12 to 0.57 cm^2 V^{-1} s^{-1}.[142] The efficient charge transport properties of **1j** were attributed to its superior molecular ordering in the thin film. Similarly, perfluorophenyl substituted NDI derivative **1k** exhibits significantly higher mobilities of 0.87 and 0.31 cm^2 V^{-1} s^{-1} under vacuum and in air, respectively, along with a high current on/off ratio of 10^7, corroborating that n-type mobility is influenced simultaneously by thermodynamic and kinetic factors.[146]

Substitution of the NDI core with halogen atoms yields NDI derivatives with low LUMO levels. Dichlorinated NDI based molecular semiconductors **1l** and **1m** with different fluoroalkyl chains show identical LUMO energy levels of −4.01 eV.[139,147] Compound **1l** exhibits electron mobilities of 0.86 and 0.91 cm^2 V^{-1} s^{-1} and high current on/off ratios of the order 10^5–10^6 in N$_2$ and air, indicating its excellent ambient device stability.[139] An excellent mobility of 4.26 cm^2 V^{-1} s^{-1} was observed for **1l** thin film FET devices deposited using the solvent shearing method under bias stress applied for one thousand cycles.[148] In air, a superior charge carrier mobility of 8.6 cm^2 V^{-1} s^{-1} is obtained when micro ribbon shaped single crystal FET devices are fabricated from **1l**.[147,149] The mobility reduces by 13% (7.5 cm^2 V^{-1} s^{-1}) when the device is stored in air for 82 days. A very high electron mobility for **1l** was afforded

because the *c*-axis, which is the crystal growth as well as the π-stacking direction, coincides with the transport direction. Low LUMO level and dense molecular packing (ρ = 2.046 g cm^{-3}) due to close π–π and fluoroalkyl chain stacking render an ideal combination of thermodynamic and kinetic stability of the molecular anion against environmental oxidation. An interesting observation reported for compound **1l** by the same research group is that the electron mobility and air stability vary between α and β-phases. In both phases, the crystal growth direction is the same, but due to lower electronic coupling in the β-phase, a lower mobility of 3.5 cm^2 V^{-1} s^{-1} compared to 8.6 cm^2 V^{-1} s^{-1} in the α-phase is observed. Nonetheless, the β-phase shows better ambient stability (5% degradation after 3 months) than the α-phase. A single crystal packing diagram and device stability in the α-and β-phases are shown in Fig. 4.

Compound **1m** shows excellent thin film transistor (TFT) device stability with an electron mobility of 1.43 cm^2 V^{-1} s^{-1} in air and a slightly reduced mobility of 1.26 cm^2 V^{-1} s^{-1} in N$_2$.[139] Both **1l** and **1m** retained 80% of their device mobility while stored for three months under ambient conditions. These dichloro substituted NDIs exhibit high field-effect mobilities due to very short π–π stacking distances of 3.3–3.4 Å, large π-stack overlap and high density in the crystalline state (2.046–2.091 g cm^{-3}).

Core fluorination or bromination does not lower the LUMO energy level as significantly as cyanation. The LUMO level of NDI derivative **1n** is lowered to −4.5 eV by introducing two cyano groups at the core of the NDI molecule.[58,150] A highly ambient stable TFT mobility of 0.11 cm^2 V^{-1} s^{-1} with a relatively low current on/off ratio of 10^3 was obtained from **1n**.[58] The high off state current measured for the FET device from **1n** might be due to unintentional doping as observed for OSCs with very low lying LUMO energy levels. Five months after device fabrication, the n-channel mobility recorded for **1n** devices under ambient conditions was slightly lower than that originally recorded under vacuum (0.15 cm^2 V^{-1} s^{-1}). Ladder type NDI derivatives were synthesized to improve the n-channel charge carrier mobility and air stability. Compound **1o**, one of the smallest ladder type NDI derivatives with a LUMO energy level of −3.79 eV, exhibits an electron mobility of 0.35 cm^2 V^{-1} s^{-1} under vacuum and a slightly reduced but stable mobility value of 0.10 cm^2 V^{-1} s^{-1} in ambient air.[151]

In recent years, donor–acceptor (D–A) type NDI derivatives have received steady attention due to their high n-channel

This journal is © The Royal Society of Chemistry 2017

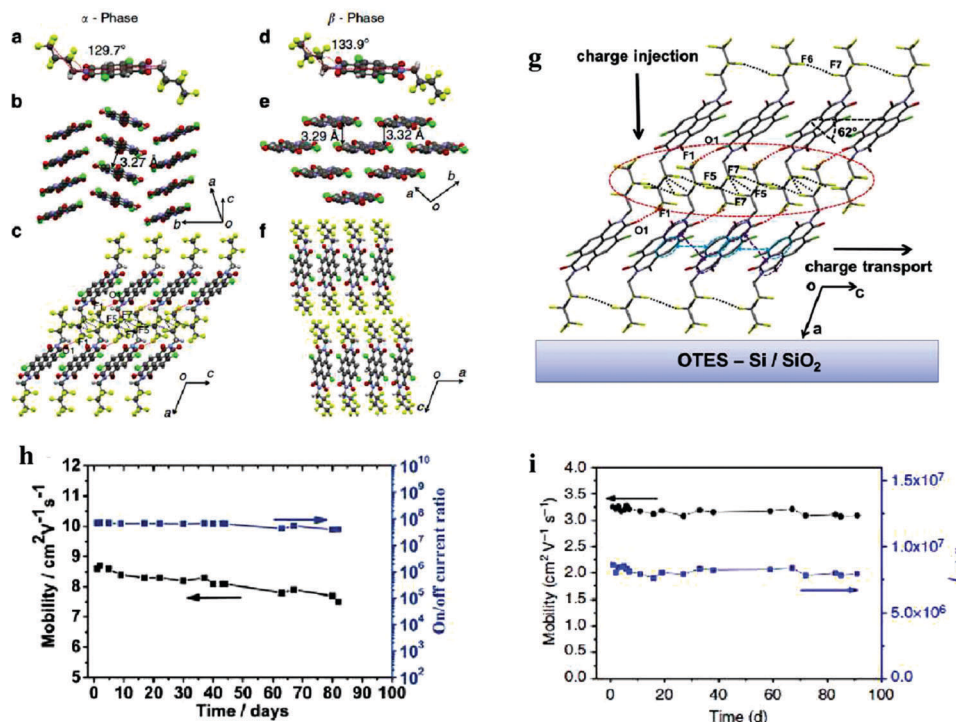*J. Mater. Chem. C*, 2017, **5**, 7404–7430 | **7411**

Fig. 4 Crystal structure of compound **1l** in the α- and β-phase in three perpendicular directions (a–f). Schematic representation of the charge transport direction and the orientation of ribbon shaped micro-crystals from **1l** in the α-phase over the OTES modified Si/SiO₂ substrate (g). Ambient device stability in the α- and β-phase (h and i) respectively (adapted from ref. 147 and 149).

thin-film mobility and environmental stability. Zhu and co-workers were first to develop core-expanded NDI derivatives using new molecular design strategies,[152] *i.e.* (i) expansion of π-conjugation to promote intermolecular π–π stacking and/or S···S interactions; and (ii) incorporation of end-capped electron-withdrawing groups (like CN) to lower the LUMO energies. The general structure of core expanded NDI derivatives is shown in Fig. 3. Gao *et al.* reported a core-expanded NDI derivative (**1′a**) by fusing 2-(1,3-dithiol-2-ylidene)malonitrile with a tetrabromo NDI core.[152] A solution processed thin film from **1′a** affords an electron mobility of 0.51 cm² V⁻¹ s⁻¹ under ambient conditions. Further structural and device optimization led to significant improvement of the electron transport properties and air stability. The n-type mobility and current on/off ratio are enhanced to 1.2 cm² V⁻¹ s⁻¹ and 10⁷, respectively, with pentafluorobenzenethiol (PFBT) treatment of the bottom-contact gold electrodes.[74] The high ambient stability of **1′a** is due to its very low LUMO energy level of −4.36 eV. The mobility was further increased to 3.5 cm² V⁻¹ s⁻¹ by tuning the branching position and the *N*-alkyl chain length.[84] The best n-channel mobility was observed for compound **1′b** with chain branching two carbon atoms away from the conjugated backbone.[84] X-ray diffraction revealed that changes in the branching position modify solid state molecular packing leading to alteration in the grain size and thin film morphology. Compound **1′b** shows efficient packing and large grain size which leads to one of the best solution processed thin film electron mobilities with air stability.

Laterally extended naphtho[2,3-*b*:6,7-*b′*]dithiophenediimide (NDTI) derivatives show rise in the HOMO level which imparts ambipolarity. Core functionalization of NDTI derivatives with

electron withdrawing substituents such as chloro (**1′c**), or 5-pyrimidyl (**1′d**) groups, helps maintaining lower HOMO and LUMO levels and improves structural organization.[153] Interestingly, chloro substitution at the α-positions of NDTI derivatives leads to favourable molecular packing through intermolecular Cl···O=C interactions. **1′c** crystallizes with bricklayer 2D packing due to additional Cl···O=C interactions. Theoretical calculations corroborate the increase in orbital overlap between neighbouring molecules after chlorine substitution. Consequently, for **1′c**, the n-channel charge carrier mobility under ambient conditions significantly improves to 0.73 cm² V⁻¹ s⁻¹. The environmental stability of **1′c** is evident from the fact that after four months of storage in air, the charge carrier mobility decreased only marginally to 0.3 cm² V⁻¹ s⁻¹. Due to the absence of favourable interactions, a relatively low electron mobility of 0.025 cm² V⁻¹ s⁻¹ is observed for **1′d** in open air.

Using a modified synthetic procedure, several NDI derivatives with asymmetrically expanded cores were synthesized by Chen *et al.*[154] The best n-channel OTFT mobility of 0.17 cm² V⁻¹ s⁻¹ with a current on/off ratio of 10⁶ was measured for compound **1′e**. Devices fabricated from compounds **1′e** are more stable in air than the others due to their lower LUMO energy levels. Core-expanded NDI derivative **1′f** with two different *N*-alkyl substituents was reported by Hu *et al.* but it shows similar air stable n-channel performance.[155] The hetero-polycyclic based NDI derivative **1′g** with a very low LUMO energy level (−4.72 eV) was developed by Xie *et al.*[156] It exhibits a high n-channel mobility of 0.96 cm² V⁻¹ s⁻¹ under ambient conditions. Relatively high mobility and excellent environmental stability of the

compound **1′g** under low voltage operation were utilized for developing an ink-jet printed TFT device which is a step forward towards using organic materials for printed electronics. π-Conjugation was further increased by linking two NDIs with a π-bridge to synthesize compound **1′h** which shows excellent n-channel transport both in N_2 and under ambient conditions, affording an electron mobility of 0.17 cm^2 V^{-1} s^{-1}.[157] The stability of top-gate OTFT devices was assayed by employing spin-coating and ink-jet printing techniques using CYTOP and Al_2O_3 as dielectric layers.

Like NDI derivatives, small molecules based on PDI have potential in terms of n-channel charge carrier mobility and device stability. Perylene diimide, a derivative of rylene dyes, can be substituted at the imide- and at the lateral bay- and non-bay positions. The structures and substitution positions of rylene diimide molecules are shown in Fig. 5 together with chemical structures of high electron mobility PDI derivatives.

PDI derivative **2a** with C_8H_{17} chains at the imide position shows field effect mobility of 1.7 cm^2 V^{-1} s^{-1} under H_2 atmosphere (partial pressure of 10^{-4} Torr) employing SiO_2 as a dielectric (Table 2).[158] Modifying the SiO_2 dielectric by surface coating with polymethylmethacrylate (PMMA) or cyclic olefin copolymers (COC) improves air stability by reducing the concentration of trap states and results in open air mobilities of 0.36 cm^2 V^{-1} s^{-1} and 0.67 cm^2 V^{-1} s^{-1}, respectively.[159] Using gelatin as a dielectric material, the open air OTFT mobility is enhanced to 0.74 cm^2 V^{-1} s^{-1} from 0.22 cm^2 V^{-1} s^{-1} under vacuum.[160] This rise in mobility is due to an increase in the dielectric capacitance under ambient conditions. A field-effect mobility of about 0.6 cm^2 V^{-1} s^{-1} and a large current on/off ratio of 10^7 are achieved under vacuum for a thin film transistor made of N-$C_{13}H_{27}$ substituted **2b** which has a LUMO energy level of −3.4 eV.[72] A slightly higher open air electron mobility (0.69 cm^2 V^{-1} s^{-1}) and a high current on/off ratio of 10^8 are achieved with **2b**, when the gold source–drain electrodes are

modified with a 2 nm layer of thermally evaporated elemental sulfur.[72] A high n-channel charge carrier mobility of 2.1 cm^2 V^{-1} s^{-1} under vacuum was reported by Ichikawa et al. for a thin film device made with compound **2b** after improving the thin film morphology by annealing at 140 °C.[161] The mobility completely diminishes when tested in air because the LUMO level of **2b** is too high.

Fluorinated alkyl chains at the N-atoms in PDI molecules improve air stability by preventing oxygen and moisture from penetrating into the thin film and reacting with the molecular backbone. This can be explained by the larger van der Waals radius of fluorine compared to that of hydrogen which reduces the available space between the N,N'-chains from ∼4 Å to ∼2 Å in both NDI and PDI derivatives (Fig. 6).[58,134] While compounds **2c** and **2e** with CH_2CF_3 and $CH_2C_4F_9$ show moderate n-channel mobilities of 0.044/0.02 and 0.11/0.09 cm^2 V^{-1} s^{-1} under vacuum/ in air, respectively, compound **2d** with partially fluorinated alkyl chains of intermediate length ($CH_2C_3F_7$) exhibits the best n-channel charge carrier mobility of 1.44/1.24 cm^2 V^{-1} s^{-1} under vacuum/in air among the three PDI derivatives.[162] This is due to the closest packing combined with the highest planarity of **2d**. Hence, dense molecular packing enhances the charge carrier mobility in two ways, by influencing the intermolecular orbital overlap and by preventing the ingress of oxygen and water vapour.

Perfluorinated phenyl ethyl substituted PDI compound **2g** shows higher mobility (0.37 cm^2 V^{-1} s^{-1}) in open air than non-fluorinated **2f** (0.11 cm^2 V^{-1} s^{-1}).[162,163] However, a single nanowire made of **2f** demonstrates a superior mobility of 1.4 cm^2 V^{-1} s^{-1} in air.[164] A very high electron mobility of 1.13 cm^2 V^{-1} s^{-1} was also reported by Yu et al. for **2f**.[165]

Substitution at the core significantly alters the LUMO level of PDI derivatives which in turn affects their charge carrier mobility. Tetrachloro core substituted PDI derivative **2h** without N-substitution has a relatively decent mobility of 0.18 cm^2 V^{-1} s^{-1} under ambient conditions.[163] After storage in air for 80 days, the mobility decreases to 0.04 cm^2 V^{-1} s^{-1}. **2i** and **2j** with core
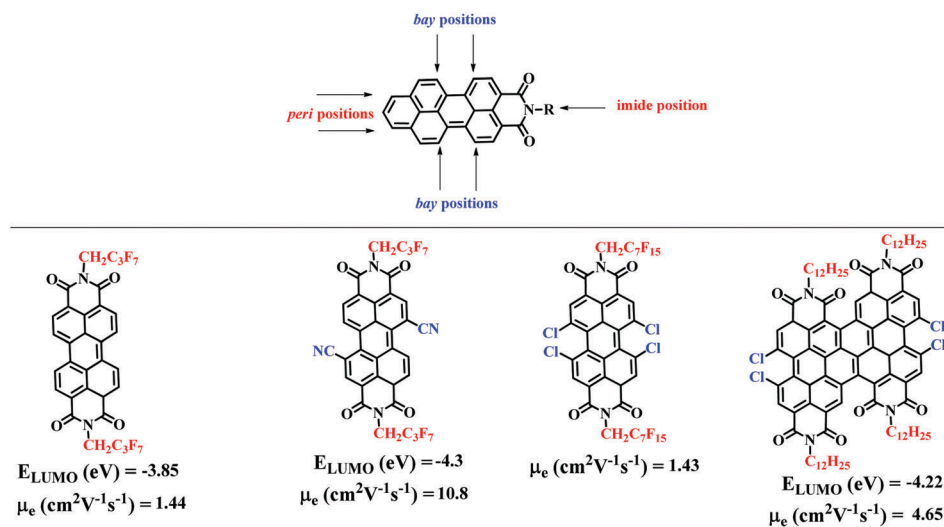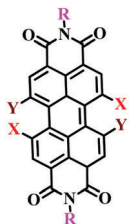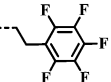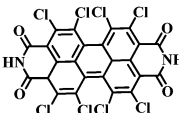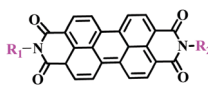

Fig. 5 Different substitution positions of a perylene molecule are indicated. The chemical structure and mobility value of high performing PDI molecules with varied imide and lateral functional groups are shown at the bottom.

This journal is © The Royal Society of Chemistry 2017

J. Mater. Chem. C, 2017, 5, 7404–7430 | 7413

Table 2 Structure and n-channel device parameters for PDI based derivatives

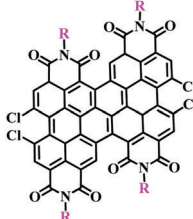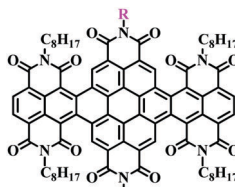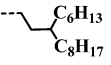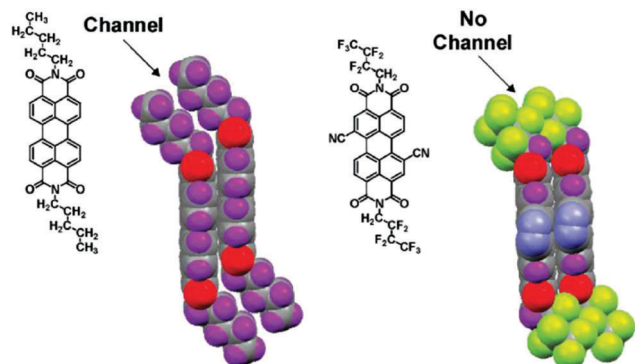| Chemical structures		R	X	Y	E_{LUMO} (eV)	μ (cm² V⁻¹ s⁻¹)	$I_{on/off}$	Device structures	Ref.
	2a	C_8H_{17}	H	H		1.7 (H_2)	10⁷	BGTC; Ag; Si/SiO₂	158
						0.36 (air)	10⁵	BGTC; Au; Si/SiO₂; PMMA	159
						0.67 (air)	10⁵	BGTC; Au; Si/SiO₂; COC	159
						0.74 (air)	10⁵	BGTC; Au; Au/gelatin	160
	2b	$C_{13}H_{27}$	H	H	−3.4	0.69 (air)	10⁸	BGTC; Au; Si/SiO₂; S/OTS	72
						2.1 (vacuum)	10⁵	BGTC; Au; Si/SiO₂	161
	2c	CH_2CF_3	H	H		0.044 (N_2)	10⁶	BGTC; Au; Si/SiO₂; OTS	162
						0.02 (air)	10⁷		
	2d	$CH_2C_3F_7$	H	H	−3.85	1.44 (N_2)	10⁶	BGTC; Au; Si/SiO₂; OTS	162
						1.24 (air)	10⁶		
	2e	$CH_2C_4F_9$	H	H	−3.84	0.11 (vacuum)	10⁶	BGTC; Au; Si/SiO₂; OTS	162
						0.12 (air)	10⁶		
	2f	(benzyl)	H	H	−4.26	0.11 (air)	10⁵	BGTC; Au; Si/SiO₂; OTS	163
					−4.39	1.4 (nanowire, air)	10⁵	BGTC; Au; Si/SiO₂; OTS	164
	2g	(pentafluorobenzyl)	H	H	−3.79	0.62 (vacuum)	10⁶	BGTC; Au; Si/SiO₂; OTS	162
						0.37 (air)	10⁷		
	2h	H	Cl	Cl	−3.9	0.18 (air)	10⁶	BGTC; Au; Si/SiO₂; OTS	163
	2i	$CH_2C_3F_7$	F	H	−3.88	0.66 (N_2)	10⁶	BGTC; Au; Si/SiO₂; OTS	162
						0.61 (air)	10⁶		
	2j	$CH_2C_3F_7$	F	F	−3.93	0.058 (N_2)	10⁶	BGTC; Au; Si/SiO₂; OTS	162
						0.056 (air)	10⁶		
	2k	(pentafluorobenzyl)	F	H	−3.94	0.85 (N_2)	10⁷	BGTC; Au; Si/SiO₂; OTS	162
						0.51 (air)	10⁷		
	2l	(pentafluorobenzyl)	Cl	Cl	−4.11	0.38 (N_2)	10⁷	BGTC; Au; Si/SiO₂; OTS	162
						0.27 (air)			
	2m	C_8H_{17}	Cl	Cl		0.8 (air)	10⁵	BGTC; Au; Si/SiO₂; OTS	167
	2n	$CH_2C_7F_{15}$	Cl	Cl		1.43 (air)	10⁷	BGTC; Au; Si/SiO₂; OTS	167
	2o	(cyclohexyl)	CN	H	−4.33	0.86 (air)	10⁷	BGTC; Au; Si/SiO₂; OTS	168
	2p	$CH_2C_3F_7$	CN	H	−4.3	6 (sc, vacuum)	10⁴	BGBC; Au; Si/SiO₂/PMMA	170
						3 (sc, air)	10⁴		
						10.8 (vacuum) (230 K)		Vacuum gap	173
						5.1 (vacuum) (290 K)			
	2q				−4.23	0.91 (vacuum)	10⁸	BGTC; Au; Si/SiO₂; OTS	175
						0.82 (air)	10⁷		
		R_1	R_2						
	2r	(2-ethylhexyl: C_2H_5, C_4H_9)	$CH_2C_3F_7$		−3.8	1.2 (sc, air)	10⁵	BGTC; Au; Si/SiO₂/PS	66
	2s	$C_{12}H_{25}$				4.65 (sc, air)		BGTC; Ag; Si/SiO₂; OTS	176
	2t	$C_{18}H_{37}$			−4.3	0.7 (air)	10⁷	BGTC; Au; Si/SiO₂; OTMS	177
	2u	(C_6H_{13}, C_8H_{17})			−4.2	0.44 (air)	10⁶	BGTC; Au; Si/SiO₂; OTS	178

MA: polymethylmethacrylate, COC: cyclic olefin copolymer.

fluorination show lower LUMO levels (**2i**: −3.88 eV and **2j**: −3.93 eV) than **2d** (−3.85 eV) with the same *N*-substitution, but the n-channel mobilities are lower for **2i** (0.66/0.61 cm² V⁻¹ s⁻¹ under vacuum/in air) and **2j** (0.058/0.056 cm² V⁻¹ s⁻¹ under

Fig. 6 Close molecular packing in the fluorinated PDI derivative as obtained from the space-filling model using the reported crystal structure (adapted from ref. 58).

vacuum/in air) than for **2d**.[162] **2d** has a slip-stacked face-to-face molecular packing with high coplanarity, while **2i** is planar but crystallizes with a herringbone arrangement. **2j** is completely distorted due to fluorine–fluorine repulsion resulting in poor π-conjugation and consequently poor charge carrier mobility.

A DFT investigation of PDI based systems with R = alkyl or fluoroalkyl, and with halogens at the bay positions reproduced the experimental findings.[166] The electron mobility of compound **2i** calculated using Marcus theory is the highest, 0.514 cm^2 V^{-1} s^{-1}. This value closely agrees with the experimental one of 0.66 cm^2 V^{-1} s^{-1} (Table 2). Introducing four fluorine atoms (compound **2j**) increases the EA but leads to a twisted structure which is detrimental for charge transport. In addition to improving the stability of the anions, electron-withdrawing substituents at the appropriate positions enhance electronic coupling which leads to an increase in mobility despite increasing λ. With their strong UV-visible absorptions[166] these materials might be excellent replacements for fullerenes in solar cells.

With the perfluorinated phenyl (C$_6$F$_5$) groups at the amide position in compound **2k** instead of the partially perfluorinated alkyl chains (CH$_2$C$_3$F$_7$), the mobility values (0.85/0.51 cm^2 V^{-1} s^{-1} in N$_2$/air) do not change much.[162] In contrast to **2j** where tetrafluoro substitution decreases electron mobility, **2l**, a tetrachloro substituted PDI derivative shows enhanced n-channel transport. This can be explained by the presence of perfluorinated phenyl (C$_6$F$_5$) groups at the N-atoms that improve molecular packing in the thin film as confirmed from single crystal structure determination.[162]

Liu *et al.* compared the single crystal OFET characteristics of two tetrachlorinated PDI derivatives (**2m** and **2n**) with non-fluorinated and fluorinated N-alkyl substituents.[167] Introduction of fluorinated alkyl chains almost doubles the open air electron mobility to 1.43 cm^2 V^{-1} s^{-1} for compound **2n** concomitantly increasing the current on/off ratio. In agreement with Katz *et al.*,[134] they speculated that fluorinated alkyl chains induce compact crystal packing which hinders the penetration of oxygen and moisture. Like halogen substitution, core cyanation of PDI derivatives can be used to create air stable n-channel OSCs. **2o** containing cyclohexyl substituents exhibits very low LUMO levels of −4.33 eV, which transpires into highly stable ambient air

mobilities of 0.86 cm^2 V^{-1} s^{-1} with a very high current on/off ratio of 10^7.[168] The open air device stability of **2o** is directly related to the active layer thickness. PDI derivative **2p** with fluroalkyl chains represents one of the best air-stable n-channel OSCs developed to date.[58,70,169–173] A low LUMO energy level of −4.3 eV and dense molecular packing improve the stability and render an open air OTFT mobility of 1.3 cm^2 V^{-1} s^{-1}.[171] Very high charge carrier mobilities of 6 and 3 cm^2 V^{-1} s^{-1} under vacuum and in open air, respectively, were achieved using a single crystal OFET device of **2p**.[170] In a vacuum-gap single-crystal OFET, an excellent mobility of 5.1 cm^2 V^{-1} s^{-1} was measured with **2p** at T = 290 K.[173] This value increases to 10.8 cm^2 V^{-1} s^{-1} at T = 230 K, indicating band-like electron transport. This was the first time that band-like transport was observed for an n-channel OFET. The charge transport properties of several core-cyanated PDI derivatives including **2p** were studied by Weitz *et al.* to analyze the effect of different fluorinated N-substituents on the air stability of OFET devices.[172] Compound **2p** was observed to have the highest n-channel charge carrier mobility among molecules with different linear or cyclic fluorinated substituents.

The effect of cyano substituents at the bay positions was compared to that of fluorine and fluorinated alkyl chains using a tunneling enabled hopping model. The molecular parameters were calculated using DFT and transport was modelled by kinetic Monte Carlo simulations.[174] Cyano groups were found to reduce λ by enhancing the delocalization of the electrons and by inducing π-stacking favourable for electron transport.[174] The calculated electron mobility of 16.96 cm^2 V^{-1} s^{-1} for **2p** (Table 2) overestimates the experimental value of 10.8 cm^2 V^{-1} s^{-1}.[173] Overestimation of the observed values is actually expected as calculations are done on idealized systems. The charge carrier mobility decreases with increasing temperature, although λ is much larger than the electron coupling. This phenomenon was attributed to tunneling enabled hopping of a localized charge that is strongly coupled with a high frequency vibrational mode.[174]

In comparison with **2l**, an octachloroperylene diimide derivative **2q** was synthesized by Wurthner and co-workers.[175] The vacuum deposited bottom-gate top-contact FET devices show comparable performances under vacuum (0.91 cm^2 V^{-1} s^{-1}) and in air (0.82 cm^2 V^{-1} s^{-1}) with very large current on/off ratios of 10^7–10^8. The much improved stability of **2q** is indicated by the retention of the electron mobility (0.6 cm^2 V^{-1} s^{-1}) even after 20 months under ambient air. Dense molecular packing and a low lying LUMO level (−4.23 eV) provide kinetic and thermodynamic stability for the molecular anions against oxidation. Recently, another high performing asymmetrically N-substituted PDI derivative **2r** was reported by Mondal *et al.*[66] Single crystals from **2r** grown on a polystyrene (PS) modified Si/SiO$_2$ substrate afford an impressive n-channel mobility of 1.2 cm^2 V^{-1} s^{-1} and a current on/off ratio of 10^5 in air. For compound **2r**, the mobility varies with the variation of the dielectric used for device fabrication. The reduction in the number of surface traps due to the hydrophobic PS coating is believed to be responsible for achieving the high electron mobility under ambient conditions.

In a new design strategy, high electron affinity and improved device stability were attained by increasing π-conjugation and functionalizing the PDI core with electron withdrawing groups. The fused bis-PDI derivatives, **2s** and **2t** with different alkyl chains, show air stable n-channel charge transport due to their low LUMO energy levels.[176,177] Single crystal devices from **2s** exhibit a high n-channel mobility of 4.65 cm^2 V^{-1} s^{-1} under ambient conditions using Ag as source-drain electrodes to align the work function of the metal electrodes with the LUMO of the OSC at −4.22 eV.[176] No serious degradation was observed when keeping the devices in air for one and half months. Similarly, **2t** with an identical π-conjugated backbone, but different solubilizing alkyl groups, shows an open air electron mobility as high as 0.7 cm^2 V^{-1} s^{-1} with an excellent on/off ratio of the order 10^7.[177] As compared to **2s** and **2t**, Xiao et al. established that **2u** with a greater laterally π-extended motif is more planar and consequently has improved open air electron mobility.[178]

Along with NDI and PDI derivatives, a few other aromatic diimide based OSCs were also found to exhibit n-channel characteristics. Among several N-substituted pyromellitic diimides (PyDI), the smallest rylene diimide, **3a** with fluoroalkyl side chains and a LUMO energy of −3.9 eV, shows a decent electron mobility of 0.079 cm^2 V^{-1} s^{-1} under vacuum, but the mobility decreases when the devices are exposed to air.[179] After 15 minutes of air exposure the mobility drops to 0.056 cm^2 V^{-1} s^{-1}. Enhancement of the electron mobility upon replacing oxygen with sulfur was found in the PyDI derivative.[180] Under ambient conditions, the thionated PyDI derivative **3′a** shows an impressive electron mobility and a current on/off ratio of 0.62 cm^2 V^{-1} s^{-1} and 10^5, respectively. The incorporation of sulfur stabilizes the LUMO, increases electronic coupling and reduces λ of diimide compounds resulting in improvement in open air n-channel mobility. To lower the LUMO level, cyano groups were introduced into the molecular backbone of anthracene and pentacene based diimide derivatives achieving ambient stability of the n-channel charge transport. The dicyano-anthracene diimide based derivatives **3b** and **3c** with alkyl and fluoroalkyl chains show an air stable electron mobility of 0.03/0.02 and 0.06/0.04 cm^2 V^{-1} s^{-1} under vacuum/in air, respectively.[181,182]

Like dicyanoanthracene diimide, a quite stable electron mobility of 0.08/0.07 cm^2 V^{-1} s^{-1} under vacuum/in air was achieved with the pentacene derivative **3d** which has a low LUMO level of −4.15 eV.[183] Tetracyano substituted coronene diimide (**3e**) is stable under ambient conditions due to its very low LUMO energy (−4.22 eV) and exhibits an open air n-channel thin film mobility of 0.16 cm^2 V^{-1} s^{-1}.[184] Wu and co-workers reported large π-conjugated dicyano substituted ovalene diimide **3f**, exhibiting unipolar transport with n-channel mobility of 1.0 cm^2 V^{-1} s^{-1} in a nitrogen atmosphere.[185] Under ambient conditions due to oxygen doping, the mobility decreases to 0.051 cm^2 V^{-1} s^{-1} with the appearance of ambipolar characteristics. Bowl-shaped single crystals of cyano substituted corannulene imides **3g** and **3h** with linear and branched N-alkyl chains exhibit air-stable electron transport in bottom-gate top-contact FET devices with mobilities of 0.07 and 0.04 cm^2 V^{-1} s^{-1}, respectively.[186] Although the LUMOs of **3g** and **3h** lie relatively high at −3.63 eV, ambient stability is provided by short intermolecular distances and dense packing

of molecules. Chemical structures and OFET performance parameters for non-NDI and PDI derivatives are summarized in Table 3.

Coronene and the effect of halogenation on 1-dimensional electron and hole transport were studied using Marcus theory. Coronenes assemble in π-stacks with short intermolecular distances of 3.0–3.3 Å and dimer binding energies of 20–30 kcal mol^{-1}. Fluorination was found to increase the reorganization energies and to decrease the mobility slightly.[124] Diimide substitution[187] (compound **3e**) increases the EAs and bathochromically shifts the low energy absorption. The reorganization energies of electrons (λ^-) and holes (λ^+) increase with diimide substitution. In all cases λ^- is greater than λ^+. With the exception of the tetradiimide, charge transfer integrals are larger for holes than for electrons and the electron mobilities were found to be 15 times smaller than the hole mobilities.[187] However, some charge transfer integrals for holes are larger than the reorganization energies, which means that hole transport is overestimated by using Marcus theory in these systems.[43]

4.2 Cyano and/or keto derivatives

Functionalization with cyano or keto groups is a powerful means to lower the LUMO energy level of π-conjugated OSCs. Fig. 7 shows various cyano or keto derivatives with very high electron mobilities. In 1994, very weak n-channel activity of the order of 10^{-5} cm^2 V^{-1} s^{-1} was observed for the first time for a cyano based compound, 7,7,8,8-tetracyanoquinodimethane (TCNQ).[188] Subsequently, Uemura et al. fabricated an air-stable single crystal FET device from TCNQ (**4a**) with a high electron mobility of 0.5 cm^2 V^{-1} s^{-1} (Table 4).[189]

Recently, the difluorinated TCNQ derivative **4b** has demonstrated an unprecedented electron mobility of 25 cm^2 V^{-1} s^{-1} at 150 K in a vacuum-gap single crystal FET device.[190] The room temperature mobility ranges from 6–7 cm^2 V^{-1} s^{-1} and the mobility increases upon lowering the temperature. The band-like charge transport observed for **4b** at low temperature is believed to arise from a unique unit cell structure with face-to-face molecular packing. This results in 3D electronic coupling and enhanced charge delocalization as reflected in the large conduction band width. TCNQ (**4a**) and its tetrafluorinated derivative do not exhibit the same extraordinary behaviour due to dynamical disorder. TCNQ forms the basic structural unit of cyano terminated quinoidal derivatives foreshowing great promise of a new class of n-channel OSCs. In recent years, a great number of air stable n-channel OFETs was devised containing OSCs with cyanovinyl units. Compound **4c**, a quinoidal thieno derivative, end-capped with dicyanomethylene groups shows a mobility of 0.16 cm^2 V^{-1} s^{-1} in ambient air.[191] Takimiya and his group introduced terminal (alkyloxycarbonyl)cyanomethylene substituents in a series of quinoidal thiophene derivatives to lower the LUMO energies and to enhance the solubility.[192] The effect of increasing π-conjugation on the charge carrier mobility in dicyanomethylene systems is reflected in compound **4d**.[193] It exhibits an open air electron mobility of 0.57 cm^2 V^{-1} s^{-1}. Two dimensional π-expanded quinoidal oligothiophenes with proximal (**4e**) and distal (**4f**) regio-chemistry, terminated with

Table 3 Structure and n-channel device parameters for non-NDI and non-PDI derivatives

Chemical structures		R	E_{LUMO} (eV)	μ (cm^2 V^{-1} s^{-1})	$I_{on/off}$	Device structures	Ref.
	3a	$CH_2CH_2C_8F_{17}$	−3.9	0.079 (vacuum) 0.056 (air)	10^6 10^5	BGTC; Au; Si/SiO$_2$; OTS	179
	3′a	$CH_2C_3F_7$	−4.18	0.62 (air)	10^5	BGTC; Au; Si/SiO$_2$; ODTS	180
	3b	C_8H_{17}	−4.07	0.03 (vacuum) 0.02 (air)	10^6 10^7	BGTC; Au; Si/SiO$_2$; HMDS	181
	3c	$CH_2C_3F_7$	−4.1	0.06 (vacuum) 0.04 (air)	105 10^4	BGTC; Au; Si/SiO$_2$; HMDS	182
	3d	C_6H_{13} C_8H_{17}	−4.15	0.08 (vacuum) 0.07 (air)	10^7 10^6	BGTC; Au; Si/SiO$_2$; OTS	183
	3e	C_8H_{17} $C_{10}H_{21}$	−4.22	0.16 (air)	10^4	TGBC; Au; Si/SiO$_2$/CYTOP	184
	3f	$C_{12}H_{25}$ $C_{10}H_{21}$	−3.9	1.0 (N$_2$) 0.51 (air)	10^5 10^4	BGTC; Au; Si/SiO$_2$; OTMS	185
	3g	C_6H_{13}	−3.62	0.07 (air)	10^4	BGTC; Au; Si/SiO$_2$/PS	186
	3h	C_2H_5 C_4H_9	−3.63	0.04 (air)	10^3	BGTC; Au; Si/SiO$_2$/PS	186

PS: polystyrene.
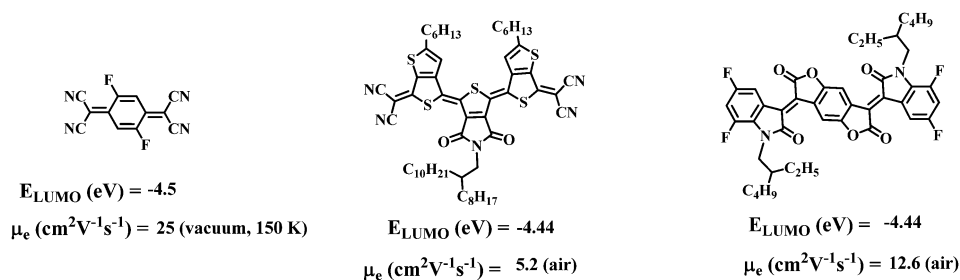
Fig. 7 High performance cyano and keto based n-channel organic semiconductors.

dicyanomethylene, show efficient n-channel ambient mobilities with a high current on/off ratio on the order of 10^6.[194] Different orientations of the thiophene rings in **4e** and **4f** result in morphology changes. As a result **4e** shows an excellent mobility of 3.0 cm^2 V^{-1} s^{-1} while its regio-isomer **4f** has a lower mobility of 0.44 cm^2 V^{-1} s^{-1}. Investigation of the effect of the nature of the alkyl chain on the charge carrier mobilities of **4e** and **4g** revealed that the branched alkyl chains in **4g** lead to one order of magnitude higher charge carrier mobility than linear alkyl

chains.[195] The higher mobility can be attributed to improved molecular packing. Single crystal data show that compound **4g** has cofacial solid state packing, whereas molecules with a similar π-backbone but with linear alkyl chains pack in a herringbone fashion. Molecule **4g** shows one of the best open air electron mobilities of 5.2 cm^2 V^{-1} s^{-1}. An excellent mobility of 0.9 cm^2 V^{-1} s^{-1} was achieved with a drop-cast film prepared from the quinoid dicyanomethylene-substituted fused tetra-thieno derivative **4h** in ambient air.[196] Li *et al.* reported a mobility

This journal is © The Royal Society of Chemistry 2017

J. Mater. Chem. C, 2017, **5**, 7404–7430 | **7417**

Table 4 Structure and n-channel device parameters for cyano and keto derivatives

Chemical structures		R	E_{LUMO} (eV)	μ (cm² V⁻¹ s⁻¹)	$I_{on/off}$	Device structures	Ref.
	4a		−4.5	0.5 (sc, air)	10^2	BGBC; Au; Si/SiO₂	189
	4b		−4.5	25 (vacuum, 150 K)			190
	4c	C₆H₁₃	−4.2	0.16 (air)	10^4	BGTC; Au; Si/SiO₂; OTS	191
	4d	C₁₂H₂₅ C₁₀H₂₁	−4.39	0.57 (air)		BGTC; Au; Si/SiO₂; OTS	193
	4e	C₂H₅ C₄H₉	−4.2	3.0 (air)	10^6	BGBC; Au; Si/SiO₂; OTS	194
	4f	C₂H₅ C₄H₉	−4.2	0.44 (air)	10^3	BGBC; Au; Si/SiO₂; OTS	194
	4g	C₈H₁₇ C₁₀H₂₁	−4.44	5.2 (air)	10^6	BGBC; Au; Si/SiO₂; OTS	195
	4h	C₆H₁₃ C₈H₁₇	−4.3	0.9 (air)	10^5	BGTC; Au; Si/SiO₂; OTS	196
	4i	C₁₂H₂₅ C₁₀H₂₁	−4.33	0.22 (air)	10^5	BGTC; Au; Si/SiO₂; OTS	197
	4j	C₂H₅ C₄H₉	−4.2	0.55 (air)	10^6	BGTC; Au; Si/SiO₂; OTS	198
	4k	C₁₆H₃₃	−4.5	0.5 (air)	10^4	TGBC; Au; Al/CYTOP	199
	4l	C₁₀H₂₁ C₁₀H₂₁	−4.5	0.72 (air)	10^5	BGTC; Au; Si/SiO₂; OTS	200
	4m	C₆H₁₃ C₈H₁₇	−4.61	0.22 (air)	10^7	BGBC; Au; Si/SiO₂; OTS	201
	4n	R₁: C₁₂H₂₅ C₁₀H₂₁ R₂: C₆H₁₃	−3.6	0.16 (air)	10^4	TGBC; Ag; Al/CYTOP	202
	4o	C₆H₁₃ C₄H₉	−4.35	1.9 (air)	10^4	BGTC; Au; Si/SiO₂; OTS	203
	4p	C₁₂H₂₅	−4.32	0.16 (air)	10^8	BGTC; Au; Si/SiO₂; OTS	55

Table 4 (*continued*)

Chemical structures		R	E_{LUMO} (eV)	μ (cm^2 V^{-1} s^{-1})	$I_{on/off}$	Device structures	Ref.
	4q	C$_8$H$_{17}$ / C$_{10}$H$_{21}$	−4.19	0.11 (air)	10^8	BGTC; Au; Si/SiO$_2$; styrene	204
	4r		−4.14	0.1 (air)	10^6	BGTC; Au; Si/SiO$_2$; OTS	205
	4s	C$_6$H$_{13}$ / C$_4$H$_9$	−4.04	0.16 (air)	10^6	TGBC; Au; Ag/CYTOP	206
	4t	C$_2$H$_5$ / C$_4$H$_9$	−4.44	12.6 (air)	10^6	BGTC; Au; Si/SiO$_2$/CYTOP	208

of 0.22 cm^2 V^{-1} s^{-1} for quinoid dicyanomethylene-substituted 2,5-di(thiophene-2yl)thieno-[3,2-*b*]thieno derivative **4i** with a current on/off ratio of 10^4 measured in air.[197] Recently, Wang *et al.* reported quinoidal dicyanomethylene containing diketopyrrolopyrrole (DPP) derivatives with different *N*-alkyl substituents that exhibit unipolar electron transport characteristics.[198] Air-stable electron mobility up to 0.55 cm^2 V^{-1} s^{-1} with a current on/off ratio of 10^6 was observed for **4j** in both vapour deposited and solution processed thin films. Heeney and coworkers reported small molecule/polymer [poly(α-methyl styrene)] (PαMS) blended n-channel OTFTs made using compound **4k,** which has the same π-backbone as **4j** but different side chains.[199] It is believed that the very low LUMO energy level of −4.5 eV is responsible for the excellent stability of the top-gate bottom-contact device under ambient conditions with a high electron mobility of 0.5 cm^2 V^{-1} s^{-1}. Current on/off ratios are low, however, with values of 10^2 to 10^3. In a separate study, the branching position of the alkyl group was varied in a series of cyanovinyl substituted DPP derivatives and their electrical properties were determined.[200] The highest mobility in a bottom-gate top-contact FET device of 0.72 cm^2 V^{-1} s^{-1} was recorded for a thin film of **4l** on an OTS treated substrate after annealing at 150 °C. All compounds exhibit very low LUMO level energies of −4.5 eV. Recently, Wang *et al.* synthesized quinoidal DPP derivatives, terminated with dicyanomethylenethienothiophene and different alkyl side chains.[201] Among them, **4m** with 2-hexyldecyl side chains has an exceptionally low LUMO level of ∼4.6 eV and an ambient stable electron mobility of 0.22 cm^2 V^{-1} s^{-1} with a very high current on/off ratio of 10^7. A DPP based oligomer like small molecule **4n** with ambient stable (RH ∼ 20–40%) electron transporting properties shows the best n-channel mobility of 0.16 cm^2 V^{-1} s^{-1} after solvent and thermal annealing of the thin

film devices.[202] Even after four weeks of air exposure, the steady performances were retained.

Tricyanovinyldihydrofuran (TCF) based compound **4o** with a terminal cyanovinyl substituent shows excellent n-channel performance under ambient conditions.[203] With a LUMO level at −4.35 eV, the devices fabricated from the self-assembled microstructure of **4o** exhibit an air-stable n-type mobility of 1.9 cm^2 V^{-1} s^{-1}. Compound **4p** with the non-quinoidal acceptor indenofluorenebis(dicyanomethylene) (IFDMT) shows an efficient n-channel mobility of 0.16 cm^2 V^{-1} s^{-1} and a current on/off ratio of 10^8 in air due to its low lying LUMO energy level of −4.32 eV.[55] The mobility and current on/off ratio remain unaltered after five months under ambient conditions. Usta and co-workers have varied the position of two terminal alkyl chains in compound **4p** from β- to α,ω positions to develop a new air stable molecular semiconductor **4q** which shows liquid crystalline (LC) properties.[204] But, interestingly, at higher temperature the charge transport characteristics diminish as compared to those of devices annealed at 50 °C. This might be due to poorer thin film microstructure at the semiconductor/dielectric interface while cooling from the LC phase for the annealed samples. The best mobility of 0.11 cm^2 V^{-1} s^{-1} and a very high on/off ratio of 10^8 for low heat-treated devices demonstrate the applicability of this new molecule for fabricating air-stable room-temperature processed n-channel thin film transistors on plastic substrates. Lately, an effective molecular design was developed to achieve ambient n-channel semiconducting performances of an OSC by adding cyano and triisopropylsilylethynyl (TIPS) groups to triphenodioxazine (TPDO) cores.[205] Compound **4r** based on cyano and TIPS substituted TPDO is stable in open air with an electron mobility and a current on/off ratio of 0.1 cm^2 V^{-1} s^{-1} and 1.3 × 10^6 respectively.[205] After 30 days of storage in air,

This journal is © The Royal Society of Chemistry 2017

J. Mater. Chem. C, 2017, **5**, 7404–7430 | 7419

the mobility and current on/off ratio decrease minimally to values of 0.08 cm^2 V^{-1} s^{-1} and 4 × 10^5. A new n-channel air-stable small molecule OSC **4s** was reported by Li and co-workers exhibiting a mobility of 0.16 cm^2 V^{-1} s^{-1} under ambient conditions in a top-gate bottom-contact device.[206] Uniform thin films of compound **4s** are highly crystalline with a layer by layer lamellar crystal structure and interlayer distances of 1.71 nm as determined using X-ray diffraction (XRD) analysis. Electron mobility is enhanced significantly when electron withdrawing cyano groups are incorporated.

Pei and coworkers recently developed high performance benzodifurandione based oligo(*p*-phenylenevinylene) (BDOPV) semiconductors, derivatives of oligo(*p*-phenylenevinylene) (OPV), which show exceptionally high, ambient stable n-channel charge carrier mobilities.[207] Pei *et al.* studied the effect of fluorine substitution on the molecular packing and charge transport parameters of different BDOPV based single crystals.[208] Variation in molecular packing with changes in the number and position of fluorine atoms in the BDOPV unit leads to significant alteration in n-channel charge carrier mobilities. Fluorinated and non-fluorinated BDOPV based compounds exhibit very high n-channel mobilities >1 cm^2 V^{-1} s^{-1} in air. Environmental stability studies during which the compounds were exposed to ambient conditions for over a month confirm their superior stability. It is remarkable that all systems show very high mobility in air, irrespective of their solid state packing. One of the best electron mobilities under ambient conditions observed so far is that of tetrafluoro substituted BDOPV (F$_4$BDOPV), **4t** (Fig. 8), of 12.6 cm^2 V^{-1} s^{-1} with a current on/off ratio of 10^6. Antiparallel cofacially stacked **4t** has four

times the electron mobility of its non-fluorinated analog that stacks in a herringbone fashion. After a month in air, the mobility in single crystal devices is reduced by 20%. Thin film devices have better environmental stability as performances degrade by only 10% during storage in air for over seven months. A low LUMO level (−4.44 eV) and dense molecular packing are presumed to be responsible for the excellent air stability.

The above literature review reflects the enormous importance of cyano substitution for the electron conductivity of quinoid molecules. Effects of cyano substitution are however complex and have an interesting history. The first calculations that explored the effect of cyano substitution on conjugated systems were done using Hückel theory on polyacetylene.[209] Excellent electronic properties for planar percyanopolyacetylene were predicted but could not be verified experimentally.[210] Although percyano-polyenes with ten repeat units turned out to be more oxidizing than chlorine and reduced forms are environmentally stable, they are strongly non-planar which is detrimental for the conductivity.[210] In heterocyclic π-systems deviation from planarity is less of a problem and cyano groups can be used to switch p-channel materials to n-channel materials.

Although CN is considered to be strongly electron withdrawing, it actually does not attract electrons in the neutral ground state.[211,212] The high electron affinity of CN substituted systems is the result of π-accepting rather than inductive effects. CN has a low lying unoccupied π*-orbital which conjugates with the π-system of OSCs, polarizing the LUMO toward itself. As a result the LUMOs of cyano-substituted compounds, which only become occupied in the first excited state or after reduction, tend to be localized on the cyano substituted acceptor in aromatic systems. The localization of the LUMOs is reflected in decreased energy level splitting and reduced oscillator strengths of the first excited states, and is, of course, detrimental to intra molecular n-channel mobility. It also affects intermolecular hopping because of smaller coupling between systems with localized orbitals. As a result of the localization effect of CN described above, many cyano-substituted polymers are stable in the reduced form but have very flat conduction bands.[212–214] Theory predicts therefore limited intramolecular electron transport in these materials.[213,214] Because the valence band is delocalized, intramolecular hole transport is comparable to that of unsubstituted systems.

The effect of localization is confirmed when aromatic quaterthiophenes end-capped with dicyano and tricyanovinylene groups are compared with quinoid systems end-capped with dicyanomethylene without a vinyl spacer. Despite short π-stacking distances, electron transport was found to be poor in aromatic species. This was rationalized with spatial separation of tricyanovinylene end groups resulting in limited electron hopping transport.[215] Unexpectedly poor conductivities in aromatic dicyano-vinyl substituted oligothio-phenes that were observed despite favourable crystal structures, short stacking distances, and high EA were attributed to local dipole moments that lead to energetic disorder.[96,97] Theoretical analysis, however, suggests that localization of the LUMO contributes to the poor electron transport properties. As end-capping with dicyano-methylene groups without the vinyl groups switches the structures from aromatic to quinoid (Table 4), the order of HOMO and LUMO
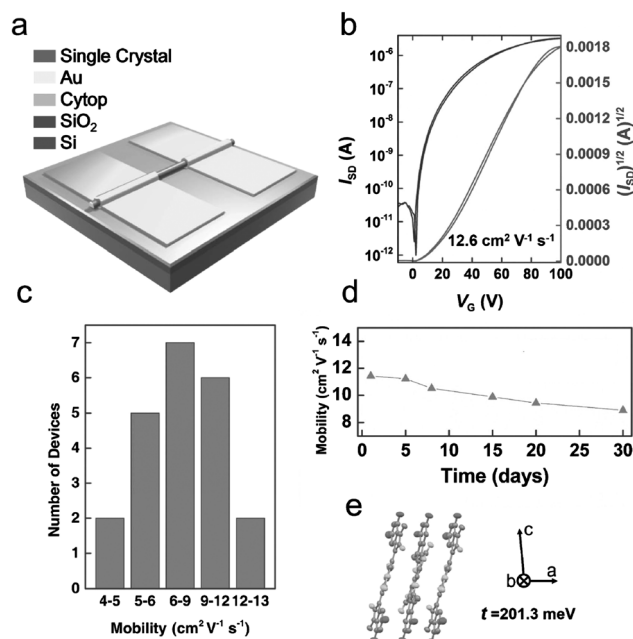

Fig. 8 The diagram for the single crystal FET device (a) and the corresponding transfer curves (b) for compound **4t**. Histogram for device performances for 22 devices (c) and the aerial stability of the FET device for a period of one month (d). (e) The transfer integral value in the π–π stacking direction (*a*-axis) (adapted from ref. 208).

7420 | *J. Mater. Chem. C*, 2017, 5, 7404–7430

This journal is © The Royal Society of Chemistry 2017

orbitals is reversed with the consequence that now the HOMO tends to be localized and the LUMO is delocalized. Consequently, charge transfer integrals for electrons are larger than for holes and electron exceeds hole mobility,[216] while aromatic cyano-vinyl end-capped thiophenes are hole conductors.[217] Hence, the quinoid nature of the small molecules (Table 4) is crucial for avoiding the detrimental localization effects otherwise observed with cyano groups.

The tendency of CN-groups to localize electrons explains experimental observations on IFDMT (compound **4p** in Table 4) which shows an excellent mobility of 0.16 cm^2 V^{-1} s^{-1}, but much lower values as the repeat unit in polymers.[55,218,219] Vapour deposited devices are better electron conductors than solution processed ones as the electron mobility decreases more than the hole mobility with disorder, indicating that electron transport is mainly inter- rather than intramolecular. Monomer crystals have high reduction potentials and can be used as electron transport materials in OFETs under ambient conditions. Excellent electron mobility (1.370 cm^2 V^{-1} s^{-1}) was predicted using Marcus theory for single crystals of a similar monomer, 2,20-(2,7-dihexy1-4,9-dihydro-*s*-indaceno[1,2-*b*:5,6-*b*0]dithiophene-4,9-diylidene)dimalononitrile.[220]
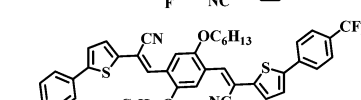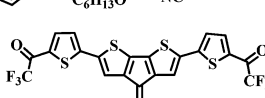
4.3 Halogen derivatives
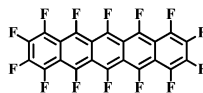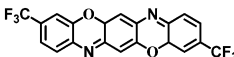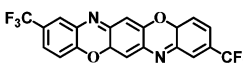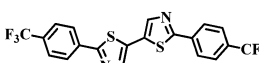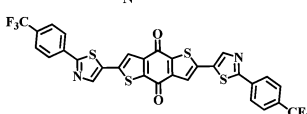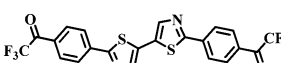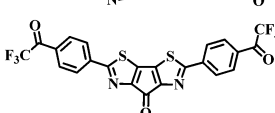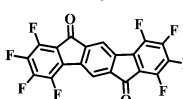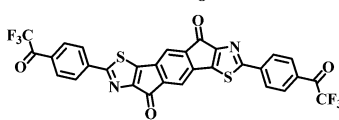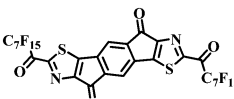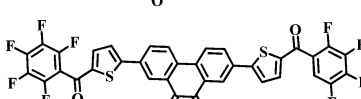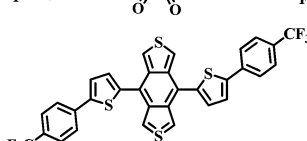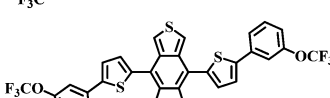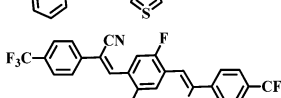
In contrast to cyano groups, halogen atoms are electron with-drawing by inductive effects and act as π-donors due to their lone pairs. The π-donating effects increase delocalization in the conduction band which is reflected in large band widths.[221–223] The idea to replace hydrogen with fluorine in conjugated systems is old.[224–226] Semi-empirical calculations predict that perfluorinated polyacetylene would be more stable than its non-fluorinated form, having a smaller band gap, higher electron mobility and better crystallinity because of the polarity of the C–F bonds.[224] DFT predicts that both IE and EA increase but that there is little change of the optical spectrum.[221] The problem with substituting the hydrogen in polyacetylene is that the larger and negatively charged fluorine substituents induce non-planarity.[221,222] Experimental work showed that perfluoropolyacetylene has increased sensitivity towards oxygen, water and light[227] as opposed to the expected stabilization. Fluorinated polypyrrole,[228] thiophene oligomers,[229] *p*-phenylene oligomers,[230] pentacene (**5a**),[231] and other heterocyclic oligomers and polymers[232–237] were synthesized and theoretical predictions of the increased stability of the n-doped state and switching from hole to electron conductivity were confirmed. In addition, fluorination has the additional benefit of promoting the air-stability of n-channel OSCs through the formation of a kinetic barrier against oxygen and moisture. The effect of fluorine on imparting electron mobility was reported by Sakamoto *et al.* for perfluorinated pentacene derivative **5a** (Table 5).[238] Pentacene shows predominantly hole mobility (μ_e: 0.020 cm^2 V^{-1} s^{-1}; μ_h: 5.0 cm^2 V^{-1} s^{-1}) while perfluoropentacene **5a** exhibits n-channel characteristics with an electron mobility of 0.11 cm^2 V^{-1} s^{-1} under vacuum. Marcus theory calculations predict that fluorinated pentacenes have almost twice the electron mobility of cyano-substituted ones despite the higher EA of the latter.[98] This can be explained by delocalization of the LUMOs with fluorine. On the down side it was found theoretically and experimentally that fluorination tends to increase λ,[231,236,239] especially for electron transport. This is believed to be caused by the spread of the LUMO electron density over the fluorine atoms.[236] A 2.5-fold increase of λ in perfluoropentacene compared to pentacene was shown using Marcus theory to reduce the hole mobility by a factor of 7.[239] The effect of fluorine substitution can also depend strongly on the position of the substitution.[240] A detailed analysis of substituent effects can be achieved by decomposing λ into contributions from internal coordinates. It was demonstrated that chlorine can be used to reduce λ when placed at appropriate positions of indolo[3,2-*b*]carbazole derivatives.[241]

Theoretical investigation of trifluoromethylation of acenes indicates that IE and EA can be influenced more than with direct backbone substitution.[242] This can be attributed to the higher number of fluorine atoms introduced but also to the lack of π-back-donation which increases orbital energies. The HOMO–LUMO gap decreases but similar to backbone substitution, λ increases. The latter effect gets smaller with increasing π-conjugation.[242] Perfluoroalkyl side chains lower the HOMO and LUMO energies by about 0.4 eV[243] which is significant as a Schottky barrier model predicts a 10^5-fold increase in the carrier injection rate when the injection barrier is lowered by 0.27 eV.[243]

Yu and co-workers reported two air stable isomers of tri-fluoromethyltriphenodioxazine **5b** and **5c**.[244] Both are n-channel materials with mobilities of 0.07 and 0.03 cm^2 V^{-1} s^{-1}, respectively. No significant decrease in the mobility was observed even after storage in air for one month. A high electron mobility of 1.83 cm^2 V^{-1} s^{-1} was observed for trifluoromethyl substituted thiazole compound **5d** on an OTS treated substrate under vacuum.[245] Ambient stability was not observed due to its small electron affinity. To enhance the electron affinity, different electron withdrawing spacers were incorporated between the two thiazole moieties of **5d** and charge transport properties were determined. The air stable n-channel OSC **5e** was developed by inserting benzo[1,2-*b*:4,5-*b'*]-dithiophene-4,8-dione into the molecular structure.[246] This derivative has a low lying LUMO level of −4.1 eV, leading to mobilities of 0.15 cm^2 V^{-1} s^{-1} under vacuum and 0.12 cm^2 V^{-1} s^{-1} in air. Bithiazole appended trifluoro-acetyl substituted **5f** is unstable under ambient conditions with weak n-channel charge transport on the order of 10^{-3} cm^2 V^{-1} s^{-1}.[247] When a carbonyl group is used to bridge the two thiazole moieties as in compound **5g**, the LUMO energy level stabilized significantly from −3.17 to −3.64 eV.[247] Introducing nitrogen into thiophene rings and employing carbonyl bridges increases EAs and therefore the stability of the n-doped state. The gain in electron affinity improves the n-channel charge carrier mobility of **5g**. In bottom-gate bottom-contact device geometry, the observed mobilities for **5g** are 0.03/0.014 cm^2 V^{-1} s^{-1} under vacuum/in air. It was observed that the mobility was not reduced after exposing the devices to air for 24 h, however, one year of exposure to an ambient environment decreases both the mobility and current on/off ratio of the device by three orders of magnitude. Although the electron mobility and current on/off ratio are partially regained under vacuum, there is a permanent increase in threshold voltage

This journal is © The Royal Society of Chemistry 2017

J. Mater. Chem. C, 2017, **5**, 7404–7430 | **7421**

Table 5 Structure and n-channel device parameters for halogen based molecules

Chemical structures		E_{LUMO} (eV)	μ (cm^2 V^{-1} s^{-1})	$I_{on/off}$	Device structures	Ref.
	5a		0.11 (vacuum)	10^2	BGBC; Au; Si/SiO$_2$	210
	5b		0.07 (air)	10^6	BGTC; Au; Si/SiO$_2$; OTS	244
	5c		0.03 (air)	10^6	BGTC; Au; Si/SiO$_2$; OTS	244
	5d	−3.67	1.83 (vacuum)	10^4	BGTC; Au; Si/SiO$_2$; OTS	245
	5e	−4.1	0.15 (vacuum) 0.12 (air)	10^3 10^4	BGTC; Au; Si/SiO$_2$; HMDS	246
	5f	−3.17	0.002 (vacuum)	10^4	BGTC; Au; Si/SiO$_2$; ODTS	247
	5g	−3.64	0.03 (vacuum) 0.014 (air)	10^3 10^4	BGTC; Au; Si/SiO$_2$; ODTS	247
	5h	−3.53	0.16 (vacuum) 0.09 (air)	10^5 10^5	BGTC; Au; Si/SiO$_2$; PS	248
	5i	−3.79	0.39 (vacuum) 0.14 (air)	10^6 10^7	BGTC; Au; Si/SiO$_2$; ODTS	249
	5j	−4.05	0.18 (vacuum) 0.09 (air)	10^7 10^7	BGBC; Au; Si/SiO$_2$; ODTS	250
	5k	−4.03	0.018 (vacuum) 0.015 (air)	10^8 10^6	BGTC; Au; Si/SiO$_2$; HMDS	251
	5l	−4.04	0.28 (vacuum) 0.16 (air)	10^3 10^5	BGTC; Au; Si/SiO$_2$; HMDS	252
	5m	−4.04	0.61 (vacuum) ∼0.61 (air)	10^6	BGTC; Au; Si/SiO$_2$; PVP	253
	5n	−4.04	0.17 (vacuum) ∼0.1 (air after 1 yr)	10^6	BGTC; Au; Si/SiO$_2$	254
	5o	−3.94	2.14 (vacuum) 0.2 (air after 1 day)	10^6	BGTC; Au; Si/SiO$_2$; OTS	255
	5p	−4.19	∼0.01 (vacuum and air)	10^5	BGTC; Au; Si/SiO$_2$; HMDS	256

which was attributed to the formation of deep trap states at the semiconductor–dielectric interface. Despite a comparatively high LUMO level (-3.64 eV), the intrinsic stability of molecular anions of **5g** arises due to the formation of a kinetic barrier against O_2/H_2O in the presence of trifluoroacetyl groups and improved crystallinity of the thin film by incorporating carbonyl groups. For indenofluorenedione **5h**, the electron mobility of 0.16 cm^2 V^{-1} s^{-1} under vacuum decreases to 0.09 cm^2 V^{-1} s^{-1} after 40 min of air exposure, but then shows negligible changes over 3 months.[248]
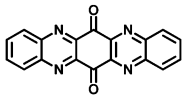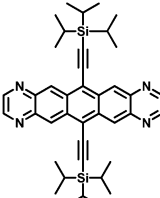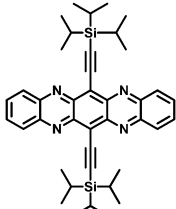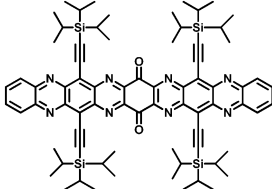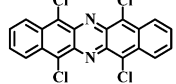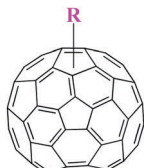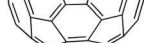
Compound **5i** with the newly designed electronegative unit of 4,9-dihydro-*s*-indaceno[1,2-*b*:5,6-*b'*]dithiazole-4,9-dione (IDD) with trifluoromethyl substituents exhibits mobilities of 0.39 and 0.14 cm^2 V^{-1} s^{-1} under vacuum and in air, respectively.[249] The open air n-channel performance of a few other IDD derivatives was studied and compound **5j** with fluorinated terminal acyl groups was observed to have relatively stable electron mobility.[250] The electron mobility of **5j** measured in air is half of that under vacuum (μ_e = 0.18 cm^2 V^{-1} s^{-1}) but the very high current on/off ratio of 10^7 is maintained. The positive effects of fluorine substitution on solid state packing, LUMO levels, and the kinetic barrier effect were confirmed. The Marks group developed the air-stable fluorine substituted phenanthrenequinone based n-channel OSC **5k** which affords mobilities of 0.018/0.015 under vacuum/in air and retention of a high current on/off ratio of 10^6.[251] Benzobis(thiadiazole) (BBT) is another strong acceptor which lowers the LUMO levels of OSCs. But air stability is achieved only when trifluoromethyl groups are introduced in the BBT derivative **5l**.[252] Under vacuum, the highest electron mobility of 0.77 cm^2 V^{-1} s^{-1} was achieved in bottom contact device geometry. In top contact devices, the mobility decreases over 50 days in air from 0.28 to 0.16 cm^2 V^{-1} s^{-1}. Mamada *et al.* reported a series of BBT derivatives among which **5m** has impressive atmospheric stability.[253] The mobility of 0.61 cm^2 V^{-1} s^{-1} measured inside a glove box remains unchanged for one month and performance reduction by 10% after half a year demonstrates its excellent ambient stability. A highly ambient stable fluorinated acrylonitrile derivative **5n** was synthesized by Nagamatsu and co-workers.[254] After exposure to air for a day, there was almost no change in the n-channel performance of an OTFT device. The mobility degrades by 40% over one year of ambient air storage. The stability of the devices improves when measured under dry air conditions. Acrylonitrile derivative **5o** was reported by Park and coworkers.[255] Under nitrogen atmosphere, the molecule exhibits a very high electron mobility of 2.14 cm^2 V^{-1} s^{-1} and a current on/off ratio of 10^6 in bottom-gate top-contact devices because of its high planarity, tight molecular stacking, high crystallinity and optimized energy levels. When tested under ambient conditions, the mobility reduces from an initial value of 1.35 cm^2 V^{-1} s^{-1} and stabilizes at 0.2 cm^2 V^{-1} s^{-1}. The air stability of the device was further improved over a test period of seven days by depositing a thin layer of NDI derivative **1g** which itself is highly stable under an open atmosphere as mentioned earlier. Compound **5p** which is structurally similar to compound **5g** demonstrates excellent ambient stable characteristics indicated by its unchanged n-channel performance after 20 cycles of operation in air.[256]

4.4 Arene and *N*-heteroarene derivatives

Introduction of nitrogen heteroatoms into conjugated frameworks increases EAs without introducing electron localization. EAs increase steadily with the number of N-atoms and it was predicted that 7–8 N-atoms are needed to increase the EA of pentacene to produce a stable n-type material.[257] Reorganization energy tends to increase as compared to that of pentacene but remains small enough, <0.2 eV, for electron transport in heptaazapentacenes with an EA of 3 eV. The EA can be increased further with terminal CN groups which additionally decrease λ to 0.132–0.160 eV.[257] N-Atoms in the backbone and CN end groups lead to an extended hydrogen bonding network that improves the crystalline order. Hence, theoretical analysis predicts that N-atoms in the π-conjugated backbone switch the charge transport properties of oligoacenes from the p-channel to the n-channel.[257,258] Oligoazaacenes have permanent dipole moments that induce switching of packing motifs from herringbone to π-stacked with short intermolecular stacking distances. Excellent electron mobilities are predicted using the Marcus theory.[102] *N*-Heteroquinones were shown to form hydrogen bonds and have the highest charge transfer integrals for hole transport along the hydrogen bonding network. Electron transport which is preferred in these materials was determined to be strongest along π-stacks.[259] Good electron mobilities of up to 0.373 cm^2 V^{-1} s^{-1} were also predicted theoretically for bisindenoanthrazolines.[260]

n-Channel charge transport characteristics were demonstrated with the incorporation of nitrogen into the backbone of insulating 6,13-pentacenequinone to form 5,7,12,14-tetraaza-6,13-pentacenequinone (**6a**) (Table 6).[261] An electron mobility of 0.12 cm^2 V^{-1} s^{-1} was measured under vacuum for **6a** while the mobility decreases by two orders of magnitude to 0.002 cm^2 V^{-1} s^{-1} when tested in air. The instability in air was attributed to the position of the LUMO energy level. To improve the electron mobility, TIPS groups were introduced at the 6 and 13 positions of tetraazapentacene derivatives in analogy with high performance p-channel 6,13-bis(triisopropylsilylethynyl)pentacene (TIPS pentacene). The positions of the N-atoms were varied from terminal (**6b**) to centre (**6c**) by Liang *et al.*[262,263] This strongly influences the LUMO energy levels and charge carrier mobilities in **6b** and **6c**. The LUMO of **6b** lies at -3.68 eV whereas it lowers to -4.01 eV in **6c**. Consequently, the best N$_2$/air mobilities in single crystal FET devices of **6b** and **6c** were determined to be 1.1/0.001 and 3.3/0.5 cm^2 V^{-1} s^{-1}. The relative improvement in mobility in **6c** in ambient air was attributed to its low LUMO level which lies in the stable electrochemical potential window for OSCs. Using a cyclohexyl terminated self-assembled monolayer (SAM) on top of a high-κ dielectric (AlO$_y$/TiO$_x$) substrate, higher n-channel charge carrier mobilities of 5 and 1.44 cm^2 V^{-1} s^{-1} were observed for thin film devices of **6c** under vacuum and in air.[264] The removal of trapped oxygen and moisture from the dielectric semiconductor interface due to hydrophobicity of the SAM is believed to be responsible for improved electron transport in the presence of air. Xu *et al.* have shown that the modification of the dielectric results in further improvement in electron mobility for **6c** both under vacuum and in air.[265]

Table 6 Structure and n-channel device parameters for arene and *N*-heteroarene derivatives

Chemical structures	R	E_{LUMO} (eV)	μ (cm^2 V^{-1} s^{-1})	$I_{on/off}$	Device structures	Ref.
	6a	−3.78	0.12 (vacuum) 0.002 (air)	10^6 10^4	BGTC; Au; Si/SiO$_2$; OTS	261
	6b	−3.68	1.1 (vacuum) 0.001 (air)		BGTC; Au; Si/SiO$_2$; OTMS	262
	6c	−4.01	13.3 (sc, N$_2$) 5.0 (vacuum) 1.44 (air) 11.1 (vacuum) 3.7 (air)	10^6 10^7	BGTC; Au; Si/SiO$_2$; BCB BGTC; Au; Si/AlO$_x$/TiO$_y$; CPDA BGTC; Au; Si/AlO$_x$/SiO$_2$; CPDA	77 264 265
	6d	−4.32	0.2 (sc, air)	10^5	BGBC; Ag; Si/SiO$_2$	266
	6e	−3.79	3.39 (sc, air)	10^4	TGTC; graphite; Si/SiO$_2$/parylene; ODTS	267
	6f		−3.63	0.25 (vacuum) 0.078 (air)	10^4	BGTC; Au; Si/SiO$_2$; HMDS	274
	6g		−3.88	0.07 (air)	10^5	BGTC; Au; Si/SiO$_2$; OTS	275
	6h		−3.85	0.51 (air)	10^4	BGTC; Au; Si/SiO$_2$; OTS	275

CPDA: 12-cyclohexyldodecylphosphonic acid.

Removal of the TiO$_x$ layer with a high quality dielectric SiO$_2$ has doubled the electron mobility to as high as 11.1 and 3.7 cm^2 V^{-1} s^{-1} under vacuum and in air, respectively, for those devices where the active material was deposited using the dip-coating method. Materials deposited through drop-casting or vacuum deposition techniques also exhibit very high n-channel mobility. But the band-like charge transport phenomenon was only observed for those devices which were fabricated using drop-casting and dip-coating methods due to the formation of highly aligned microstructures with minimum structural defects. Whereas the vacuum deposition of **6c** gives rise to mosaic-like microcrystallites having random orientation with a higher number of grain boundaries and in consequence it displays thermally activated mobility. Recently, an unprecedented n-channel mobility of 13.3 cm^2 V^{-1} s^{-1} was observed with single crystals of **6c** at room temperature under vacuum after removal of the polar solvent residues.[77] Wang *et al.* synthesized large linearly-fused

N-heteroquinones with eight sp^2 hybridized N-atoms in the backbone with the dual aim of increasing π–π* interactions for more efficient electron transport, and of lowering the LUMO level for improved air stability.[266] Single crystal FET devices with 6,10,17,21-tetra-((triisopropylsilyl)-ethynyl)-5,7,9,11,16,18,20,22-octaazanonacene-8,19-dione (**6d**) exhibit air stable electron mobilities of 0.2 cm^2 V^{-1} s^{-1} with a low LUMO energy of −4.32 eV. Using graphite as source/drain electrodes, single crystal FETs from **6e** show n-channel characteristics with a very high mobility of 3.39 cm^2 V^{-1} s^{-1} under ambient conditions.[267] Substitution of carbon with phosphorus was predicted theoretically to decrease the LUMO energies and to lead to record low reorganization energies. Therefore phospaacenes are predicted to be excellent candidates for n-channel OFETs.[268]

DFT calculations have shown that nitrogen atoms stabilize the closed-shell singlet ground state of large acenes[269] and allow tuning of the electronic structure to produce singlet-fission.[270]

7424 | *J. Mater. Chem. C*, 2017, 5, 7404–7430

This journal is © The Royal Society of Chemistry 2017

However, calculation of the correct ground state of long acenes is a complicated theoretical problem and the predictions of biradical ground states of long acenes using DFT might be artifacts.[271,272]

Fullerene and its derivatives are well-known n-type materials and are used extensively as electron acceptors in bulk hetero-junction solar cells. However, the applicability of most fullerene derivatives is limited by their high LUMO energies (*e.g.* −3.7 eV for $PC_{60}BM$) which lead to instability of the anions in air. An exception is $PC_{84}BM$ with a low lying LUMO of around −4.0 eV and the open air stability of the reduced form.[273] In spite of a LUMO level at −3.6 eV, the perfluoroalkyl-substituted C_{60} derivative **6f** shows n-channel performance with an electron mobility of 0.078 cm^2 V^{-1} s^{-1} in an open air device. This could be achieved because the dense fluorocarbon chains prevent oxidants from air penetrating into the channel.[274] Indene and *o*-xylene mono-substituted C_{60} derivatives **6g** and **6h** exhibit an air stable n-channel mobility of 0.07 and 0.51 cm^2 V^{-1} s^{-1}, respectively, which is attributed to their low LUMO energy ($\sim$ −3.8 eV).[275]

5. Conclusions

At present, the highest air stable n-channel OFET electron mobility of 12.6 cm^2 V^{-1} s^{-1} was achieved in devices made of small molecules. As these values are still lower than the hole mobilities in ultrapure single crystals, further increase can be expected in the near future.

The highest values are reached with large extended π-systems such as NDI, PDI, and azaacenes that contain fluorine atoms or fluorinated alkyl chains. Fluorine seems to be effective in increasing electron transport as π-back donation from fluorine substituents to the backbone increases delocalization of the unoccupied orbitals. Fluorinated side chains increase the EAs and stabilize the reduced state by increasing the EAs and by creating a kinetic barrier against water and oxygen penetration. Cyano substitution leads to high n-channel conductivity mainly in quinoidal small molecules. Theoretical analysis reveals that in aromatic molecules with cyano acceptors, electrons tend to be trapped because of the localization of the LUMO on the cyano groups. This problem is avoided in quinoid systems as the HOMO and LUMO are switched and localization occurs only in the HOMO.

Once materials with promising intrinsic properties are found, processing techniques play the crucial role. Thin films have to be produced with optimized growth rates. Slow rates are not necessarily best as varying rates might allow the filling of grain boundaries improving the performance. Lamellar packing and edge-on orientation on the substrate are the most efficient structural arrangements. Attention has also to be paid to the reproducibility of device fabrication and not only to locally maximal mobilities.

Mobilities of over 10 cm^2 V^{-1} s^{-1} achieved in some materials by now are already too high to be predicted by using Marcus theory because such mobility values cannot be achieved with transfer integrals that are less than half of the reorganization energy. Therefore, theoretical studies on high performing n-type materials will have to employ methods that are suitable for treating coherent transport.

Considering the recent rapid improvements in the stability and electron transport properties of recently developed organic semiconductors, the printed electronics industry will benefit and soon a growing market for a wide range of appliances is expected to develop.

Acknowledgements

References

1 H. Shirakawa, E. J. Louis, A. G. Macdiarmid, C. K. Chiang and A. J. Heeger, *J. Chem. Soc., Chem. Commun.*, 1977, 578–580.

2 C. K. Chiang, C. R. Fincher, Y. W. Park, A. J. Heeger, H. Shirakawa, E. J. Louis, S. C. Gau and A. G. Macdiarmid, *Phys. Rev. Lett.*, 1977, **39**, 1098–1101.

3 R. O. Loufty, A.-M. Hor, C.-K. Hsiao, G. Baranyi and P. Kazmaier, *Pure Appl. Chem.*, 1988, **60**, 1047–1054.

4 H. Bässler, *Adv. Mater.*, 1993, **5**, 662–665.

5 U. Mitschke and P. Bäuerle, *J. Mater. Chem.*, 2000, **10**, 1471–1507.

6 A. Kraft, A. C. Grimsdale and A. B. Holmes, *Angew. Chem., Int. Ed.*, 1998, **37**, 402–428.

7 A. C. Arias, J. D. MacKenzie, I. McCulloch, J. Rivnay and A. Salleo, *Chem. Rev.*, 2010, **110**, 3–24.

8 H. Sirringhaus, T. Kawase, R. H. Friend, T. Shimoda, M. Inbasekaran, W. Wu and E. P. Woo, *Science*, 2000, **290**, 2123–2126.

9 J. A. Rogers, T. Someya and Y. Huang, *Science*, 2010, **327**, 1603–1607.

10 J. A. Rogers, Z. Bao, K. Baldwin, A. Dodabalapur, B. Crone, V. R. Raju, V. Kuck, H. Katz, K. Amundson, J. Ewing and P. Drzaic, *Proc. Natl. Acad. Sci. U. S. A.*, 2001, **98**, 4835–4840.

11 J. A. Rogers, Z. N. Bao, A. Makhija and P. Braun, *Adv. Mater.*, 1999, **11**, 741–745.

12 Z. N. Bao, Y. Feng, A. Dodabalapur, V. R. Raju and A. J. Lovinger, *Chem. Mater.*, 1997, **9**, 1299–1301.

13 K. Fukuda, Y. Takeda, M. Mizukami, D. Kumaki and S. Tokito, *Sci. Rep.*, 2014, **4**, 3947.

14 H. Yan, Z. Chen, Y. Zheng, C. Newman, J. R. Quinn, F. Dotz, M. Kastler and A. Facchetti, *Nature*, 2009, **457**, 679–686.

15 G. Gelinck, P. Heremans, K. Nomoto and T. D. Anthopoulos, *Adv. Mater.*, 2010, **22**, 3778–3798.

16 T. N. Jackson, *Nat. Mater.*, 2005, **4**, 581–582.

17 A. R. Brown, A. Pomp, C. M. Hart and D. M. Deleeuw, *Science*, 1995, **270**, 972–974.

This journal is © The Royal Society of Chemistry 2017

J. Mater. Chem. C, 2017, **5**, 7404–7430 | 7425

18 B. Crone, A. Dodabalapur, Y. Y. Lin, R. W. Filas, Z. Bao, A. LaDuca, R. Sarpeshkar, H. E. Katz and W. Li, *Nature*, 2000, **403**, 521–523.

19 B. C. Tee, C. Wang, R. Allen and Z. Bao, *Nat. Nanotechnol.*, 2012, **7**, 825–832.

20 K.-J. Baeg, M. Caironi and Y.-Y. Noh, *Adv. Mater.*, 2013, **25**, 4210–4244.

21 A. Tsumura, H. Koezuka and T. Ando, *Appl. Phys. Lett.*, 1986, **49**, 1210–1212.

22 X. Guo, A. Facchetti and T. J. Marks, *Chem. Rev.*, 2014, **114**, 8943–9021.

23 K. Zhou, H. Dong, H. L. Zhang and W. Hu, *Phys. Chem. Chem. Phys.*, 2014, **16**, 22448–22457.

24 W. Zhang, Y. Liu and G. Yu, *Adv. Mater.*, 2014, **26**, 6898–6904.

25 H. Dong, C. Wang and W. Hu, *Chem. Commun.*, 2010, **46**, 5211–5222.

26 I. Kang, H. J. Yun, D. S. Chung, S. K. Kwon and Y. H. Kim, *J. Am. Chem. Soc.*, 2013, **135**, 14896–14899.

27 J. Lee, A. R. Han, J. Kim, Y. Kim, J. H. Oh and C. Yang, *J. Am. Chem. Soc.*, 2012, **134**, 20713–20721.

28 J. Lee, A. R. Han, H. Yu, T. J. Shin, C. Yang and J. H. Oh, *J. Am. Chem. Soc.*, 2013, **135**, 9540–9547.

29 J. Li, Y. Zhao, H. S. Tan, Y. Guo, C. A. Di, G. Yu, Y. Liu, M. Lin, S. H. Lim, Y. Zhou, H. Su and B. S. Ong, *Sci. Rep.*, 2012, **2**, 754.

30 H. Bronstein, Z. Y. Chen, R. S. Ashraf, W. M. Zhang, J. P. Du, J. R. Durrant, P. S. Tuladhar, K. Song, S. E. Watkins, Y. Geerts, M. M. Wienk, R. A. J. Janssen, T. Anthopoulos, H. Sirringhaus, M. Heeney and I. McCulloch, *J. Am. Chem. Soc.*, 2011, **133**, 3272–3275.

31 G. Kim, S.-J. Kang, G. K. Dutta, Y.-K. Han, T. J. Shin, Y.-Y. Noh and C. Yang, *J. Am. Chem. Soc.*, 2014, **136**, 9477–9483.

32 H. R. Tseng, H. Phan, C. Luo, M. Wang, L. A. Perez, S. N. Patel, L. Ying, E. J. Kramer, T. Q. Nguyen, G. C. Bazan and A. J. Heeger, *Adv. Mater.*, 2014, **26**, 2993–2998.

33 G. R. Hutchison, M. A. Ratner and T. J. Marks, *J. Am. Chem. Soc.*, 2005, **127**, 16866–16881.

34 V. Coropceanu, J. Cornil, D. A. daSilvaFilho, Y. Olivier, R. Silbey and J. L. Bredas, *Chem. Rev.*, 2007, **107**, 926–952.

35 A. R. Murphy and J. M. J. Frechet, *Chem. Rev.*, 2007, **107**, 1066–1096.

36 L. L. Chua, J. Zaumseil, J. F. Chang, E. C. Ou, P. K. Ho, H. Sirringhaus and R. H. Friend, *Nature*, 2005, **434**, 194–199.

37 P. Prins, F. C. Grozema, J. M. Schins, S. Patil, U. Scherf and L. D. Siebbeles, *Phys. Rev. Lett.*, 2006, **96**, 146601.

38 W. Warta and N. Karl, *Phys. Rev. B: Condens. Matter Mater. Phys.*, 1985, **32**, 1172–1182.

39 C. D. Dimitrakopoulos and D. J. Mascaro, *IBM J. Res. Dev.*, 2001, **45**, 11–27.

40 C. Yuan-Chung and R. J. Silbey, *J. Chem. Phys.*, 2008, **128**, 114713.

41 J. Nelson, J. J. Kwiatkowski, J. Kirkpatrick and J. M. Frost, *Acc. Chem. Res.*, 2009, **42**, 1768–1778.

42 O. Frank, B. Friedhelm and H. Karsten, *New J. Phys.*, 2010, **12**, 023011.

43 A. Troisi, *Chem. Soc. Rev.*, 2011, **40**, 2347–2358.

44 J. P. Bergfield and M. A. Ratner, *Phys. Status Solidi B*, 2013, **250**, 2249–2296.

45 F. Gajdos, H. Oberhofer, M. Dupuis and J. Blumberger, *J. Phys. Chem. Lett.*, 2013, **4**, 1012–1017.

46 B. M. Savoie, N. E. Jackson, L. X. Chen, T. J. Marks and M. A. Ratner, *Acc. Chem. Res.*, 2014, **47**, 3385–3394.

47 F. Ortmann, K. S. Radke, A. Günther, D. Kasemann, K. Leo and G. Cuniberti, *Adv. Funct. Mater.*, 2015, **25**, 1933–1954.

48 J. R. Reimers, L. K. McKemmish, R. H. McKenzie and N. S. Hush, *Phys. Chem. Chem. Phys.*, 2015, **17**, 24641–24665.

49 Z. Shuai, L. Meng and Y. Jiang, in *Progress in High-Efficient Solution Process Organic Photovoltaic Devices*, ed. Y. Yang and G. Li, Springer Berlin Heidelberg, 2015, ch. 4, vol. 130, pp. 101–142.

50 L. Wang, O. V. Prezhdo and D. Beljonne, *Phys. Chem. Chem. Phys.*, 2015, **17**, 12395–12406.

51 R. A. Street, *Science*, 2013, **341**, 1072–1073.

52 A. Babel and S. A. Jehnekhe, *Adv. Mater.*, 2002, **14**, 371–374.

53 D. M. deLeeuw, M. M. J. Simenon, A. R. Brown and R. E. F. Einerhand, *Synth. Met.*, 1997, **87**, 53–59.

54 X. Gao and Y. Hu, *J. Mater. Chem. C*, 2014, **2**, 3099–3117.

55 H. Usta, C. Risko, Z. Wang, H. Huang, M. K. Deliomeroglu, A. Zhukhovitskiy, A. Facchetti and T. J. Marks, *J. Am. Chem. Soc.*, 2009, **131**, 5586–5608.

56 I. G. Hill and A. Kahn, *Proc. SPIE*, 1998, 168.

57 H. Z. Chen, M. M. Ling, X. Mo, M. M. Shi, M. Wang and Z. Bao, *Chem. Mater.*, 2007, **19**, 816–824.

58 B. A. Jones, A. Facchetti, M. R. Wasielewski and T. J. Marks, *J. Am. Chem. Soc.*, 2007, **129**, 15259–15278.

59 Y.-C. Chang, M.-Y. Kuo, C.-P. Chen, H.-F. Lu and I. Chao, *J. Phys. Chem. C*, 2010, **114**, 11595–11601.

60 C. R. Newman, C. D. Frisbie, D. A. da Silva, J. L. Bredas, P. C. Ewbank and K. R. Mann, *Chem. Mater.*, 2004, **16**, 4436–4451.

61 H.-I. Un, Y.-Q. Zheng, K. Shi, J.-Y. Wang and J. Pei, *Adv. Funct. Mater.*, 2017, **27**, 1605058.

62 M.-H. Yoon, C. Kim, A. Facchetti and T. J. Marks, *J. Am. Chem. Soc.*, 2006, **128**, 12851–12869.

63 J. Veres, S. Ogier and G. Lloyd, *Chem. Mater.*, 2004, **16**, 4543–4555.

64 W. H. Lee, S. G. Lee, Y. J. Kwark, D. R. Lee, S. Lee and J. H. Cho, *ACS Appl. Mater. Interfaces*, 2014, **6**, 22807–22814.

65 M. Jesper, M. Alt, J. Schinke, S. Hillebrandt, I. Angelova, V. Rohnacher, A. Pucci, U. Lemmer, W. Jaegermann, W. Kowalsky, T. Glaser, E. Mankel, R. Lovrincic, F. Golling, M. Hamburger and U. H. Bunz, *Langmuir*, 2015, **31**, 10303–10309.

66 S. Mondal, W.-H. Lin, Y.-C. Chen, S.-H. Huang, R. Yang, B.-H. Chen, T.-F. Yang, S.-W. Mao and M.-Y. Kuo, *Org. Electron.*, 2015, **23**, 64–69.

67 R. P. Ortiz, A. Facchetti and T. J. Marks, *Chem. Rev.*, 2010, **110**, 205–239.

68 J. Veres, S. D. Ogier, S. W. Leeming, D. C. Cupertino and S. M. Khaffaf, *Adv. Funct. Mater.*, 2003, **13**, 199–204.

69 J. Zaumseil and H. Sirringhaus, *Chem. Rev.*, 2007, **107**, 1296–1323.

70 R. T. Weitz, K. Amsharov, U. Zschieschang, M. Burghard, M. Jansen, M. Kelsch, B. Rhamati, P. A. van Aken, K. Kern and H. Klauk, *Chem. Mater.*, 2009, **21**, 4949–4954.

71 P. M. Beaujuge and J. M. Frechet, *J. Am. Chem. Soc.*, 2011, **133**, 20009–20029.

72 Y. Wen, Y. Liu, C.-a. Di, Y. Wang, X. Sun, Y. Guo, J. Zheng, W. Wu, S. Ye and G. Yu, *Adv. Mater.*, 2009, **21**, 1631–1635.

73 A. Facchetti, M. Mushrush, H. E. Katz and T. J. Marks, *Adv. Mater.*, 2003, **15**, 33–38.

74 Y. Zhao, C.-a. Di, X. Gao, Y. Hu, Y. Guo, L. Zhang, Y. Liu, J. Wang, W. Hu and D. Zhu, *Adv. Mater.*, 2011, **23**, 2448–2453.

75 Y. Hu, X. Gao, C.-a. Di, X. Yang, F. Zhang, Y. Liu, H. Li and D. Zhu, *Chem. Mater.*, 2011, **23**, 1204–1215.

76 J. Kim, K.-J. Baeg, D. Khim, D. T. James, J.-S. Kim, B. Lim, J.-M. Yun, H.-G. Jeong, P. S. K. Amegadze, Y.-Y. Noh and D.-Y. Kim, *Chem. Mater.*, 2013, **25**, 1572–1583.

77 G. Xue, J. Xu, C. Fan, S. Liu, Z. Huang, Y. Liu, B. Shan, H. L. Xin, Q. Miao, H. Chen and H. Li, *Mater. Horiz.*, 2016, **3**, 119–123.

78 H. Yan, Y. Zheng, R. Blache, C. Newman, S. Lu, J. Woerle and A. Facchetti, *Adv. Mater.*, 2008, **20**, 3393–3398.

79 J. Rivnay, R. Steyrleuthner, L. H. Jimison, A. Casadei, Z. Chen, M. F. Toney, A. Facchetti, D. Neher and A. Salleo, *Macromolecules*, 2011, **44**, 5246–5255.

80 Y. Li, S. Chen, Q. Liu, Y. Li, Y. Shi, X. Wang, J. Ma and Z. Hu, *J. Phys. Chem. C*, 2014, **118**, 14218–14226.

81 W.-Y. Lee, J. H. Oh, S.-L. Suraru, W.-C. Chen, F. Wuerthner and Z. Bao, *Adv. Funct. Mater.*, 2011, **21**, 4173–4181.

82 H. A. Becerril, M. E. Roberts, Z. Liu, J. Locklin and Z. Bao, *Adv. Mater.*, 2008, **20**, 2588–2594.

83 J. H. Oh, W.-Y. Lee, T. Noe, W.-C. Chen, M. Koenemann and Z. Bao, *J. Am. Chem. Soc.*, 2011, **133**, 4204–4207.

84 F. Zhang, Y. Hu, T. Schuettfort, C.-a. Di, X. Gao, C. R. McNeill, L. Thomsen, S. C. B. Mannsfeld, W. Yuan, H. Sirringhaus and D. Zhu, *J. Am. Chem. Soc.*, 2013, **135**, 2338–2349.

85 J. Dhar, C. Kanimozhi, N. Yaacobi-Gross, T. D. Anthopoulos, U. Salzner and S. Patil, *Isr. J. Chem.*, 2014, **54**, 817–827.

86 M. Shahid, T. McCarthy-Ward, J. Labram, S. Rossbauer, E. B. Domingo, S. E. Watkins, N. Stingelin, T. D. Anthopoulos and M. Heeney, *Chem. Sci.*, 2012, **3**, 181–185.

87 B. J. Jung, N. J. Tremblay, M. L. Yeh and H. E. Katz, *Chem. Mater.*, 2011, **23**, 568–582.

88 S. D. Dimitrov and J. R. Durrant, *Chem. Mater.*, 2014, **26**, 616–630.

89 G. García, J. M. Granadino-Roldán, A. Hernández-Laguna, A. Garzón and M. Fernández-Gómez, *J. Chem. Theory Comput.*, 2013, **9**, 2591–2601.

90 G. J. O. Beran, S. Wen, K. Nanda, Y. Huang and Y. Heit, *Top. Curr. Chem.*, 2014, **345**, 59–98.

91 S.-H. Wen, A. Li, J. Song, W.-Q. Deng, K.-L. Han and W. A. Goddard III, *J. Phys. Chem. B*, 2009, **113**, 8813–8819.

92 M. Olson, Y. Mao, T. Windus, M. Kemp, M. Ratner, N. Léon and V. Mujica, *J. Phys. Chem. B*, 1998, **102**, 941–947.

93 Z. Li, X. Zhang, Y. Zhang, C. F. Woellner, M. Kuik, J. Liu, T.-Q. Nguyen and G. Lu, *J. Phys. Chem. C*, 2013, **117**, 6730–6740.

94 P. Kordt and D. Andrienko, *J. Chem. Theory Comput.*, 2016, **12**, 36–40.

95 C. Poelking and D. Andrienko, *J. Am. Chem. Soc.*, 2015, **137**, 6320–6326.

96 M. Schrader, C. Korner, C. Elschner and D. Andrienko, *J. Mater. Chem.*, 2012, **22**, 22258–22264.

97 M. Schrader, R. Fitzner, M. Hein, C. Elschner, B. Baumeier, K. Leo, M. Riede, P. Bauerle and D. Andrienko, *J. Am. Chem. Soc.*, 2012, **134**, 6052–6056.

98 S. Chai, S.-H. Wen, J.-D. Huang and K.-L. Han, *J. Comput. Chem.*, 2011, **32**, 3218–3225.

99 X. Wang and K.-C. Lau, *J. Phys. Chem. C*, 2012, **116**, 22749–22758.

100 D. Fazzi, M. Caironi and C. Castiglioni, *J. Am. Chem. Soc.*, 2011, **133**, 19056–19059.

101 J. A. Letizia, M. R. Salata, C. M. Tribout, A. Facchetti, M. A. Ratner and T. J. Marks, *J. Am. Chem. Soc.*, 2008, **130**, 9679–9694.

102 X.-K. Chen, J.-F. Guo, L.-Y. Zou, A.-M. Ren and J.-X. Fan, *J. Phys. Chem. C*, 2011, **115**, 21416–21428.

103 E. G. Emberly and G. Kirczenow, *Phys. Rev. B: Condens. Matter Mater. Phys.*, 1998, **58**, 10911–10920.

104 M. Di Ventra, S. T. Pantelides and N. D. Lang, *Phys. Rev. Lett.*, 2000, **84**, 979–982.

105 L. E. Hall, J. R. Reimers, N. S. Hush and K. Silverbrook, *J. Chem. Phys.*, 2000, **112**, 1510–1521.

106 R. W. Munn and R. Silbey, *J. Chem. Phys.*, 1985, **83**, 1843–1853.

107 T. Holstein, *Ann. Phys.*, 2000, **281**, 725–773.

108 T. Holstein, *Ann. Phys.*, 2000, **281**, 706–724.

109 R. A. Marcus, *Rev. Mod. Phys.*, 1993, **65**, 599.

110 F. Gajdos, S. Valner, F. Hoffmann, J. Spencer, M. Breuer, A. Kubas, M. Dupuis and J. Blumberger, *J. Chem. Theory Comput.*, 2014, **10**, 4653–4660.

111 Y. Yamashita, F. Hinkel, T. Marszalek, W. Zajaczkowski, W. Pisula, M. Baumgarten, H. Matsui, K. Müllen and J. Takeya, *Chem. Mater.*, 2016, **28**, 420–424.

112 D. Jacquemin, E. A. Perpète, I. Ciofini and C. Adamo, *Chem. Phys. Lett.*, 2005, **405**, 376–381.

113 D. Jacquemin and E. A. Perpete, *THEOCHEM*, 2007, **804**, 31–34.

114 D. Jacquemin, E. A. Perpete, M. Medved, G. Scalmani, M. Frisch, R. Kobayashi and C. Adamo, *J. Chem. Phys.*, 2007, **126**, 191108.

115 D. Jacquemin, E. A. Perpete, G. E. Scuseria, I. Ciofini and C. Adamo, *J. Chem. Theory Comput.*, 2008, **4**, 123–135.

116 D. Jacquemin, V. r. Wathelet, E. A. Perpète and C. Adamo, *J. Chem. Theory Comput.*, 2009, **5**, 2420–2435.

117 A. D. Laurent and D. Jacquemin, *Int. J. Quantum Chem.*, 2013, **113**, 2019–2039.

118 D. Jacquemin, B. Moore, A. Planchat, C. Adamo and J. Autschbach, *J. Chem. Theory Comput.*, 2014, **10**, 1677–1685.

119 U. Salzner and A. Aydin, *J. Chem. Theory Comput.*, 2011, **7**, 2568–2583.

120 C. Sutton, J. S. Sears, V. Coropceanu and J.-L. Brédas, *J. Phys. Chem. Lett.*, 2013, **4**, 919–924.

121 J. C. Sancho-Garcia, *Chem. Phys.*, 2007, **331**, 321–331.

This journal is © The Royal Society of Chemistry 2017

J. Mater. Chem. C, 2017, **5**, 7404–7430 | 7427

122 E. F. Valeev, V. Coropceanu, D. A. Da Silva Filho, S. Salman and J. L. Brédas, *J. Am. Chem. Soc.*, 2006, **128**, 9882–9886.

123 S.-H. Wen, A. Li, J. Song, W.-Q. Deng, K.-L. Han and W. A. Goddard, *J. Phys. Chem. B*, 2009, **113**, 8813–8819.

124 J. C. Sancho-García and A. J. Pérez-Jiménez, *J. Chem. Phys.*, 2014, **141**, 1–11.

125 G. Guillaud, M. A. Sadoun, M. Maitrot, J. Simon and M. Bouvet, *Chem. Phys. Lett.*, 1990, **167**, 503–506.

126 G. Horowitz, F. Kouki, P. Spearman, D. Fichou, C. Nogues, X. Pan and F. Garnier, *Adv. Mater.*, 1996, **8**, 242–245.

127 X. Zhan, A. Facchetti, S. Barlow, T. J. Marks, M. A. Ratner, M. R. Wasielewski and S. R. Marder, *Adv. Mater.*, 2011, **23**, 268–284.

128 F. Wurthner, *Chem. Commun.*, 2004, 1564–1579.

129 J. G. Laquindanum, H. E. Katz, A. Dodabalapur and A. J. Lovinger, *J. Am. Chem. Soc.*, 1996, **118**, 11331–11332.

130 C. D. Dimitrakopoulos and P. R. L. Malenfant, *Adv. Mater.*, 2002, **14**, 99–117.

131 R. J. Chesterfield, J. C. McKeen, C. R. Newman, C. D. Frisbie, P. C. Ewbank, K. R. Mann and L. L. Miller, *J. Appl. Phys.*, 2004, **95**, 6396–6405.

132 J. H. Schön, C. Kloc and B. Batlogg, *Appl. Phys. Lett.*, 2000, **77**, 3776–3778.

133 P. R. L. Malenfant, C. D. Dimitrakopoulos, J. D. Gelorme, L. L. Kosbar, T. O. Graham, A. Curioni and W. Andreoni, *Appl. Phys. Lett.*, 2002, **80**, 2517–2519.

134 H. E. Katz, A. J. Lovinger, J. Johnson, C. Kloc, T. Siegrist, W. Li, Y. Y. Lin and A. Dodabalapur, *Nature*, 2000, **404**, 478–481.

135 H. Katz, J. Johnson, A. J. Lovinger and W. Li, *J. Am. Chem. Soc.*, 2000, **122**, 7787–7792.

136 D. Natali and M. Caironi, *Adv. Mater.*, 2012, **24**, 1357–1387.

137 J. D. Yuen and F. Wudl, *Energy Environ. Sci.*, 2013, **6**, 392–406.

138 D. Shukla, S. F. Nelson, D. C. Freeman, M. Rajeswaran, W. G. Ahearn, D. M. Meyer and J. T. Carey, *Chem. Mater.*, 2008, **20**, 7486–7491.

139 J. H. Oh, S.-L. Suraru, W.-Y. Lee, M. Koenemann, H. W. Hoeffken, C. Roeger, R. Schmidt, Y. Chung, W.-C. Chen, F. Wuerthner and Z. Bao, *Adv. Funct. Mater.*, 2010, **20**, 2148–2156.

140 A. Lv, Y. Li, W. Yue, L. Jiang, H. Dong, G. Zhao, Q. Meng, W. Jiang, Y. He, Z. Li, Z. Wang and W. Hu, *Chem. Commun.*, 2012, **48**, 5154–5156.

141 B. J. Jung, K. Lee, J. Sun, A. G. Andreou and H. E. Katz, *Adv. Funct. Mater.*, 2010, **20**, 2930–2944.

142 K. C. See, C. Landis, A. Sarjeant and H. Katz, *Chem. Mater.*, 2008, **20**, 3609–3616.

143 Y. Jung, K.-J. Baeg, D.-Y. Kim, T. Someya and S. Y. Park, *Synth. Met.*, 2009, **159**, 2117–2121.

144 D. Zhang, L. Zhao, Y. Zhu, A. Li, C. He, H. Yu, Y. He, C. Yan, O. Goto and H. Meng, *ACS Appl. Mater. Interfaces*, 2016, **8**, 18277–18283.

145 L. Zhao, D. Zhang, Y. Zhu, P. Sen, H. Meng and W. Huang, *J. Mater. Chem. C*, 2017, **5**, 848–853.

146 B. J. Jung, J. Sun, T. Lee, A. Sarjeant and H. E. Katz, *Chem. Mater.*, 2009, **21**, 94–101.

147 T. He, M. Stolte and F. Wurthner, *Adv. Mater.*, 2013, **25**, 6951–6955.

148 M. Stolte, M. Gsanger, R. Hofmockel, S. L. Suraru and F. Wurthner, *Phys. Chem. Chem. Phys.*, 2012, **14**, 14181–14185.

149 T. He, M. Stolte, C. Burschka, N. H. Hansen, T. Musiol, D. Kalblein, J. Pflaum, X. Tao, J. Brill and F. Wurthner, *Nat. Commun.*, 2015, **6**, 5954.

150 B. A. Jones, A. Facchetti, T. J. Marks and M. R. Wasielewski, *Chem. Mater.*, 2007, **19**, 2703–2705.

151 R. P. Ortiz, H. Herrera, R. Blanco, H. Huang, A. Facchetti, T. J. Marks, Y. Zheng and J. L. Segura, *J. Am. Chem. Soc.*, 2010, **132**, 8440–8452.

152 X. Gao, C. A. Di, Y. Hu, X. Yang, H. Fan, F. Zhang, Y. Liu, H. Li and D. Zhu, *J. Am. Chem. Soc.*, 2010, **132**, 3697–3699.

153 M. Nakano, I. Osaka, D. Hashizume and K. Takimiya, *Chem. Mater.*, 2015, **27**, 6418–6425.

154 X. Chen, J. Wang, G. Zhang, Z. Liu, W. Xu and D. Zhang, *New J. Chem.*, 2013, **37**, 1720–1727.

155 Y. Hu, Y. Qin, X. Gao, F. Zhang, C.-a. Di, Z. Zhao, H. Li and D. Zhu, *Org. Lett.*, 2012, **14**, 292–295.

156 J. Xie, K. Shi, K. Cai, D. Zhang, J.-Y. Wang, J. Pei and D. Zhao, *Chem. Sci.*, 2016, **7**, 499–504.

157 D. K. Hwang, R. R. Dasari, M. Fenoll, V. Alain-Rizzo, A. Dindar, J. W. Shim, N. Deb, C. Fuentes-Hernandez, S. Barlow, D. G. Bucknall, P. Audebert, S. R. Marder and B. Kippelen, *Adv. Mater.*, 2012, **24**, 4445–4450.

158 R. J. Chesterfield, J. C. McKeen, C. R. Newman, P. C. Ewbank, D. A. da Silva, J. L. Bredas, L. L. Miller, K. R. Mann and C. D. Frisbie, *J. Phys. Chem. B*, 2004, **108**, 19281–19292.

159 J.-D. Oh, H.-S. Seo, D.-K. Kim, E.-S. Shin and J.-H. Choi, *Org. Electron.*, 2012, **13**, 2192–2200.

160 L.-K. Mao, J.-Y. Gan, J.-C. Hwang, T.-H. Chang and Y.-L. Chueh, *Org. Electron.*, 2014, **15**, 920–925.

161 S. Tatemichi, M. Ichikawa, T. Koyama and Y. Taniguchi, *Appl. Phys. Lett.*, 2006, **89**, 112108.

162 R. Schmidt, J. H. Oh, Y.-S. Sun, M. Deppisch, A.-M. Krause, K. Radacki, H. Braunschweig, M. Koenemann, P. Erk, Z. Bao and F. Wuerthner, *J. Am. Chem. Soc.*, 2009, **131**, 6215–6228.

163 M.-M. Ling, P. Erk, M. Gomez, M. Koenemann, J. Locklin and Z. Bao, *Adv. Mater.*, 2007, **19**, 1123–1127.

164 J. H. Oh, H. W. Lee, S. Mannsfeld, R. M. Stoltenberg, E. Jung, Y. W. Jin, J. M. Kim, J. B. Yoo and Z. Bao, *Proc. Natl. Acad. Sci. U. S. A.*, 2009, **106**, 6065–6070.

165 H. Yu, Z. Bao and J. H. Oh, *Adv. Funct. Mater.*, 2013, **23**, 629–639.

166 S. Chai, S.-H. Wen and K.-L. Han, *Org. Electron.*, 2011, **12**, 1806–1814.

167 C. Liu, C. Xiao, Y. Li, W. Hu, Z. Li and Z. Wang, *Chem. Commun.*, 2014, **50**, 12462–12464.

168 J. H. Oh, Y.-S. Sun, R. Schmidt, M. F. Toney, D. Nordlund, M. Koenemann, F. Wuerthner and Z. Bao, *Chem. Mater.*, 2009, **21**, 5508–5518.

169 B. A. Jones, M. J. Ahrens, M. H. Yoon, A. Facchetti, T. J. Marks and M. R. Wasielewski, *Angew. Chem., Int. Ed.*, 2004, **43**, 6363–6366.

170 A. S. Molinari, H. Alves, Z. Chen, A. Facchetti and A. F. Morpurgo, *J. Am. Chem. Soc.*, 2009, **131**, 2462–2463.

7428 | *J. Mater. Chem. C*, 2017, **5**, 7404–7430

This journal is © The Royal Society of Chemistry 2017

171 J. Soeda, T. Uemura, Y. Mizuno, A. Nakao, Y. Nakazawa, A. Facchetti and J. Takeya, *Adv. Mater.*, 2011, **23**, 3681–3685.

172 R. T. Weitz, K. Amsharov, U. Zschieschang, E. B. Villas, D. K. Goswami, M. Burghard, H. Dosch, M. Jansen, K. Kern and H. Klauk, *J. Am. Chem. Soc.*, 2008, **130**, 4637–4645.

173 N. A. Minder, S. Ono, Z. Chen, A. Facchetti and A. F. Morpurgo, *Adv. Mater.*, 2012, **24**, 503–508.

174 L. Lin, H. Geng, Z. Shuai and Y. Luo, *Org. Electron.*, 2012, **13**, 2763–2772.

175 M. Gsanger, J. H. Oh, M. Konemann, H. W. Hoffken, A. M. Krause, Z. Bao and F. Wurthner, *Angew. Chem., Int. Ed.*, 2010, **49**, 740–743.

176 A. Lv, S. R. Puniredd, J. Zhang, Z. Li, H. Zhu, W. Jiang, H. Dong, Y. He, L. Jiang, Y. Li, W. Pisula, Q. Meng, W. Hu and Z. Wang, *Adv. Mater.*, 2012, **24**, 2626–2630.

177 J. Zhang, L. Tan, W. Jiang, W. Hu and Z. Wang, *J. Mater. Chem. C*, 2013, **1**, 3200–3206.

178 C. Xiao, W. Jiang, X. Li, L. Hao, C. Liu and Z. Wang, *ACS Appl. Mater. Interfaces*, 2014, **6**, 18098–18103.

179 Q. Zheng, J. Huang, A. Sarjeant and H. E. Katz, *J. Am. Chem. Soc.*, 2008, **130**, 14410–14411.

180 T.-F. Yang, S.-H. Huang, Y.-P. Chiu, B.-H. Chen, Y.-W. Shih, Y.-C. Chang, J.-Y. Yao, Y.-J. Lee and M.-Y. Kuo, *Chem. Commun.*, 2015, **51**, 13772–13775.

181 H. Usta, C. Kim, Z. Wang, S. Lu, H. Huang, A. Facchetti and T. J. Marks, *J. Mater. Chem.*, 2012, **22**, 4459–4472.

182 Z. Wang, C. Kim, A. Facchetti and T. J. Marks, *J. Am. Chem. Soc.*, 2007, **129**, 13362–13363.

183 J. Chang, H. Qu, Z.-E. Ooi, J. Zhang, Z. Chen, J. Wu and C. Chi, *J. Mater. Chem. C*, 2013, **1**, 456–462.

184 C. Zhang, K. Shi, K. Cai, J. Xie, T. Lei, Q. Yan, J. Y. Wang, J. Pei and D. Zhao, *Chem. Commun.*, 2015, **51**, 7144–7147.

185 J. Li, J.-J. Chang, H. S. Tan, H. Jiang, X. Chen, Z. Chen, J. Zhang and J. Wu, *Chem. Sci.*, 2012, **3**, 846–850.

186 R. Chen, R. Q. Lu, K. Shi, F. Wu, H. X. Fang, Z. X. Niu, X. Y. Yan, M. Luo, X. C. Wang, C. Y. Yang, X. Y. Wang, B. Xu, H. Xia, J. Pei and X. Y. Cao, *Chem. Commun.*, 2015, **51**, 13768–13771.

187 S. Sanyal, A. K. Manna and S. K. Pati, *J. Phys. Chem. C*, 2013, **117**, 825–836.

188 A. R. Brown, D. M. Deleeuw, E. J. Lous and E. E. Havinga, *Synth. Met.*, 1994, **66**, 257–261.

189 M. Yamagishi, Y. Tominari, T. Uemura and J. Takeya, *Appl. Phys. Lett.*, 2009, **94**, 053305.

190 Y. Krupskaya, M. Gibertini, N. Marzari and A. F. Morpurgo, *Adv. Mater.*, 2015, **27**, 2453–2458.

191 S. Handa, E. Miyazaki, K. Takimiya and Y. Kunugi, *J. Am. Chem. Soc.*, 2007, **129**, 11684–11685.

192 Y. Suzuki, E. Miyazaki and K. Takimiya, *J. Am. Chem. Soc.*, 2010, **132**, 10453–10466.

193 J. Li, X. Qiao, Y. Xiong, H. Li and D. Zhu, *Chem. Mater.*, 2014, **26**, 5782–5788.

194 C. Zhang, Y. Zang, E. Gann, C. R. McNeill, X. Zhu, C.-a. Di and D. Zhu, *J. Am. Chem. Soc.*, 2014, **136**, 16176–16184.

195 C. Zhang, Y. Zang, F. Zhang, Y. Diao, C. R. McNeill, C.-a. Di, X. Zhu and D. Zhu, *Adv. Mater.*, 2016, **28**, 8456–8462.

196 Q. Wu, R. Li, W. Hong, H. Li, X. Gao and D. Zhu, *Chem. Mater.*, 2011, **23**, 3138–3140.

197 Q. Wu, S. Ren, M. Wang, X. Qiao, H. Li, X. Gao, X. Yang and D. Zhu, *Adv. Funct. Mater.*, 2013, **23**, 2277–2284.

198 Y. Qiao, Y. Guo, C. Yu, F. Zhang, W. Xu, Y. Liu and D. Zhu, *J. Am. Chem. Soc.*, 2012, **134**, 4084–4087.

199 H. Zhong, J. Smith, S. Rossbauer, A. J. P. White, T. D. Anthopoulos and M. Heeney, *Adv. Mater.*, 2012, **24**, 3205–3211.

200 C. Wang, Y. Qin, Y. Sun, Y.-S. Guan, W. Xu and D. Zhu, *ACS Appl. Mater. Interfaces*, 2015, **7**, 15978–15987.

201 C. Wang, Y. Zang, Y. Qin, Q. Zhang, Y. Sun, C. A. Di, W. Xu and D. Zhu, *Chem. – Eur. J.*, 2014, **20**, 13755–13761.

202 T. Mukhopadhyay, B. Puttaraju, S. P. Senanayak, A. Sadhanala, R. Friend, H. A. Faber, T. D. Anthopoulos, U. Salzner, A. Meyer and S. Patil, *ACS Appl. Mater. Interfaces*, 2016, **8**, 25415–25427.

203 H. A. Um, J. H. Lee, H. Baik, M. J. Cho and D. H. Choi, *Chem. Commun.*, 2016, **52**, 13012–13015.

204 R. Ozdemir, D. Choi, M. Ozdemir, H. Kim, S. T. Kostakoğlu, M. Erkartal, H. Kim, C. Kim and H. Usta, *ChemPhysChem*, 2017, **18**, 850–861.

205 G. Gruntz, H. Lee, L. Hirsch, F. Castet, T. Toupance, A. L. Briseno and Y. Nicolas, *Adv. Electron. Mater.*, 2015, **1**, 1500072.

206 W. Hong, C. Guo, B. Sun, Z. Yan, C. Huang, Y. Hu, Y. Zheng, A. Facchetti and Y. Li, *J. Mater. Chem. C*, 2013, **1**, 5624–5627.

207 J. H. Dou, Y. Q. Zheng, Z. F. Yao, T. Lei, X. Shen, X. Y. Luo, Z. A. Yu, S. D. Zhang, G. Han, Z. Wang, Y. Yi, J. Y. Wang and J. Pei, *Adv. Mater.*, 2015, **27**, 8051–8055.

208 J. H. Dou, Y. Q. Zheng, Z. F. Yao, Z. A. Yu, T. Lei, X. Shen, X. Y. Luo, J. Sun, S. D. Zhang, Y. F. Ding, G. Han, Y. Yi, J. Y. Wang and J. Pei, *J. Am. Chem. Soc.*, 2015, **137**, 15947–15956.

209 S. M. Abdelaty and H. Fukutome, *Prog. Theor. Phys.*, 1986, **75**, 1283–1294.

210 H. Yu, G. Srdanov, H. Hasharoni and F. Wudl, *Tetrahedron*, 1997, **53**, 15593–15602.

211 U. Salzner and T. Kiziltepe, *J. Org. Chem.*, 1999, **64**, 764–769.

212 U. Salzner, J. B. Lagowski, R. A. Poirier and P. G. Pickup, *J. Org. Chem.*, 1999, **64**, 7419–7425.

213 U. Salzner and M. E. Köse, *J. Phys. Chem. B*, 2002, **106**, 9221–9226.

214 U. Salzner, *J. Chem. Theory Comput.*, 2014, **10**, 4921–4937.

215 M. W. Burand, K. A. McGee, X. Cai, D. A. da Silva Filho, J. L. Brédas, C. Daniel Frisbie and K. R. Mann, *Chem. Phys. Lett.*, 2006, **425**, 251–256.

216 G. Wang, Y. Kan, Y. Geng, Y. Duan, L. Wang, H. Wu, X. Dong and Z. Su, *Theor. Chem. Acc.*, 2014, **133**, 1–8.

217 T. G. Erbay, V. Aviyente and S. Salman, *Synth. Met.*, 2015, **210**(Part B), 236–244.

218 H. Usta, A. Facchetti and T. J. Marks, *J. Am. Chem. Soc.*, 2008, **130**, 8580–8581.

219 H. Usta, A. Facchetti and T. J. Marks, *Acc. Chem. Res.*, 2011, **44**, 501–510.

220 H.-L. Wei and Y.-F. Liu, *Appl. Phys. A: Mater. Sci. Process.*, 2014, **116**, 1711–1717.

This journal is © The Royal Society of Chemistry 2017

J. Mater. Chem. C, 2017, **5**, 7404–7430 | 7429

221 U. Salzner, *J. Phys. Chem. B*, 2003, **107**, 1129–1134.

222 U. Salzner, *Synth. Met.*, 2003, **135–136**, 311–312.

223 U. Salzner, *J. Phys. Chem. A*, 2010, **114**, 5397–5405.

224 T. Yamabe, K. Tanaka, H. Terama-E, K. Fukui, H. Shirakawa and S. Ikeda, *Synth. Met.*, 1980, **1**, 321–327.

225 S. M. Abdelaty and H. Fukutome, *Prog. Theor. Phys.*, 1986, **75**, 1265–1282.

226 A. K. Bakhshi, J. Ladik and C.-M. Liegener, *Synth. Met.*, 1987, **20**, 43–55.

227 G. L. Gould, V. Eswara, R. M. Trifu and D. G. Castner, *J. Am. Chem. Soc.*, 1999, **121**, 3781.

228 P. Audebert, F. Miomandre, S. G. Di Magno, V. V. Smirnov and P. Hapiot, *Chem. Mater.*, 2000, **12**, 2025–2030.

229 Y. Sakamoto, S. Komatsu and T. Suzuki, *J. Am. Chem. Soc.*, 2001, **123**, 4643–4644.

230 S. B. Heidenhain, Y. Sakamoto, T. Suzuki, A. Miura, H. Fujikawa, T. Mori, S. Tokito and Y. Taga, *J. Am. Chem. Soc.*, 2000, **122**, 10240–10241.

231 H.-Y. Chen and I. Chao, *Chem. Phys. Lett.*, 2005, **401**, 539–545.

232 F. C. Krebs and M. Jørgensen, *Macromolecules*, 2002, **35**, 7200–7206.

233 A. Facchetti, J. Letizia, M.-H. Yoon, M. Mushrush, H. E. Katz and T. J. Marks, *Chem. Mater.*, 2004, **16**, 4715–4727.

234 M.-H. Yoon, A. Facchetti, C. E. Stern and T. J. Marks, *J. Am. Chem. Soc.*, 2006, **128**, 5792–5801.

235 Y. Ie, M. Nitani, M. Ishikawa, K.-I. Nakayama, H. Tada, T. Kaneda and Y. Aso, *Org. Lett.*, 2007, **9**, 2115–2118.

236 L. T. Ming and Z. Bao, *Chem. Mater.*, 2011, **23**, 446–455.

237 A. Facchetti, M.-H. Yoon, C. L. Stern, H. E. Katz and T. J. Marks, *Angew. Chem., Int. Ed.*, 2003, **42**, 3900–3903.

238 Y. Sakamoto, T. Suzuki, M. Kobayashi, Y. Gao, Y. Fukai, Y. Inoue, F. Sato and S. Tokito, *J. Am. Chem. Soc.*, 2004, **126**, 8138–8140.

239 S. Kera, S. Hosoumi, K. Sato, H. Fukagawa, S.-i. Nagamatsu, Y. Sakamoto, T. Suzuki, H. Huang, W. Chen, A. T. S. Wee, V. Coropceanu and N. Ueno, *J. Phys. Chem. C*, 2013, **117**, 22428–22437.

240 H. J. Son, W. Wang, T. Xu, Y. Liang, Y. Wu, G. Li and L. Yu, *J. Am. Chem. Soc.*, 2011, **133**, 1885–1894.

241 H. Geng, Y. Niu, Q. Peng, Z. Shuai, V. Coropceanu and J.-L. Brédas, *J. Chem. Phys.*, 2011, **135**, 104703.

242 H. Sun, A. Putta and M. Billion, *J. Phys. Chem. A*, 2012, **116**, 8015–8022.

243 A. Facchetti, M. Mushrush, M.-H. Yoon, G. R. Hutchison, M. A. Ratner and T. J. Marks, *J. Am. Chem. Soc.*, 2004, **126**, 13859–13874.

244 C. A. Di, J. Li, G. Yu, Y. Xiao, Y. Guo, Y. Liu, X. Qian and D. Zhu, *Org. Lett.*, 2008, **10**, 3025–3028.

245 S. Ando, R. Murakami, J. Nishida, H. Tada, Y. Inoue, S. Tokito and Y. Yamashita, *J. Am. Chem. Soc.*, 2005, **127**, 14996–14997.

246 M. Mamada, D. Kumaki, J. Nishida, S. Tokito and Y. Yamashita, *ACS Appl. Mater. Interfaces*, 2010, **2**, 1303–1307.

247 Y. Ie, M. Nitani, M. Karakawa, H. Tada and Y. Aso, *Adv. Funct. Mater.*, 2010, **20**, 907–913.

248 Y.-I. Park, J. S. Lee, B. J. Kim, B. Kim, J. Lee, D. H. Kim, S.-Y. Oh, J. H. Cho and J.-W. Park, *Chem. Mater.*, 2011, **23**, 4038–4044.

249 Y. Ie, M. Ueta, M. Nitani, N. Tohnai, M. Miyata, H. Tada and Y. Aso, *Chem. Mater.*, 2012, **24**, 3285–3293.

250 Y. Ie, C. Sato, M. Nitani, H. Tada and Y. Aso, *Chem. – Eur. J.*, 2014, **20**, 16509–16515.

251 J. A. Letizia, S. Cronin, R. P. Ortiz, A. Facchetti, M. A. Ratner and T. J. Marks, *Chem. – Eur. J.*, 2010, **16**, 1911–1928.

252 T. Kono, D. Kumaki, J. Nishida, S. Tokito and Y. Yamashita, *Chem. Commun.*, 2010, **46**, 3265–3267.

253 M. Mamada, H. Shima, Y. Yoneda, T. Shimano, N. Yamada, K. Kakita, T. Machida, Y. Tanaka, S. Aotsuka, D. Kumaki and S. Tokito, *Chem. Mater.*, 2015, **27**, 141–147.

254 S. Nagamatsu, S. Oku, K. Kuramoto, T. Moriguchi, W. Takashima, T. Okauchi and S. Hayase, *ACS Appl. Mater. Interfaces*, 2014, **6**, 3847–3852.

255 S. W. Yun, J. H. Kim, S. Shin, H. Yang, B.-K. An, L. Yang and S. Y. Park, *Adv. Mater.*, 2012, **24**, 911–915.

256 M. H. Yoon, S. A. Dibenedetto, A. Facchetti and T. J. Marks, *J. Am. Chem. Soc.*, 2005, **127**, 1348–1349.

257 M. Winkler and K. N. Houk, *J. Am. Chem. Soc.*, 2007, **129**, 1805–1815.

258 U. H. F. Bunz, J. U. Engelhart, B. D. Lindner and M. Schaffroth, *Angew. Chem., Int. Ed.*, 2013, **52**, 3810–3821.

259 G. Yang, Y. Si, Y. Geng, F. Yu, Q. Wu and Z. Su, *Theor. Chem. Acc.*, 2011, **128**, 257–264.

260 X.-Y. Zhang and G.-J. Zhao, *J. Phys. Chem. C*, 2012, **116**, 13858–13864.

261 Q. Tang, Z. Liang, J. Liu, J. Xu and Q. Miao, *Chem. Commun.*, 2010, **46**, 2977–2979.

262 Z. Liang, Q. Tang, R. Mao, D. Liu, J. Xu and Q. Miao, *Adv. Mater.*, 2011, **23**, 5514–5518.

263 Z. Liang, Q. Tang, J. Xu and Q. Miao, *Adv. Mater.*, 2011, **23**, 1535–1539.

264 D. Liu, Z. He, Y. Su, Y. Diao, S. C. Mannsfeld, Z. Bao, J. Xu and Q. Miao, *Adv. Mater.*, 2014, **26**, 7190–7196.

265 X. Xu, Y. Yao, B. Shan, X. Gu, D. Liu, J. Liu, J. Xu, N. Zhao, W. Hu and Q. Miao, *Adv. Mater.*, 2016, **28**, 5276–5283.

266 C. Wang, J. Zhang, G. Long, N. Aratani, H. Yamada, Y. Zhao and Q. Zhang, *Angew. Chem., Int. Ed.*, 2015, **54**, 6292–6296.

267 M. M. Islam, S. Pola and Y. T. Tao, *Chem. Commun.*, 2011, **47**, 6356–6358.

268 G. Long, X. Yang, W. Chen, M. Zhang, Y. Zhao, Y. Chen and Q. Zhang, *Phys. Chem. Chem. Phys.*, 2016, **18**, 3173–3178.

269 G. Junkuo and Z. Qichun, *Isr. J. Chem.*, 2014, **54**, 699–702.

270 S. Ito and M. Nakano, *J. Phys. Chem. C*, 2015, **119**, 148–157.

271 C. U. Ibeji and D. Ghosh, *Phys. Chem. Chem. Phys.*, 2015, **17**, 9849–9856.

272 D. H. Ess, E. R. Johnson, X. Hu and W. Yang, *J. Phys. Chem. A*, 2011, **115**, 76–83.

273 T. D. Anthopoulos, F. B. Kooistra, H. J. Wondergem, D. Kronholm, J. C. Hummelen and D. M. de Leeuw, *Adv. Mater.*, 2006, **18**, 1679–1684.

274 M. Chikamatsu, A. Itakura, Y. Yoshida, R. Azumi and K. Yase, *Chem. Mater.*, 2008, **20**, 7365–7367.

275 H. Yu, H.-H. Cho, C.-H. Cho, K.-H. Kim, D. Y. Kim, B. J. Kim and J. H. Oh, *ACS Appl. Mater. Interfaces*, 2013, **5**, 4865–4871.

7430 | *J. Mater. Chem. C*, 2017, **5**, 7404–7430

This journal is © The Royal Society of Chemistry 2017